Treating linear molecule HCCH in calculations of rotation-vibration spectra

Katy L. Chubb, Andrey Yachmenev, Jonathan Tennyson, and Sergei N. Yurchenko

Citation: The Journal of Chemical Physics **149**, 014101 (2018); doi: 10.1063/1.5031844
View online: https://doi.org/10.1063/1.5031844
View Table of Contents: http://aip.scitation.org/toc/jcp/149/1
Published by the American Institute of Physics

Treating linear molecule HCCH in calculations of rotation-vibration spectra

Katy L. Chubb,[1,a)] Andrey Yachmenev,[2] Jonathan Tennyson,[1] and Sergei N. Yurchenko[1,b)]
[1]*Department of Physics and Astronomy, University College London, London WC1E 6BT, United Kingdom*
[2]*Center for Free-Electron Laser Science (CFEL), Deutsches Elektronen-Synchrotron DESY, Notkestrasse 85, 22607 Hamburg, Germany*

(Received 31 March 2018; accepted 14 June 2018; published online 2 July 2018)

Special treatment is required for ro-vibrational calculations involving polyatomic molecules of linear geometry in order to avoid singularities in the kinetic energy operator. Here we present a variational approach which allows calculations involving such configurations, with a set of $3N-5$ linearized coordinates used to represent the vibrations. This approach has been implemented as part of the variational nuclear motion program TROVE (Theoretical ROVibrational Energies). A symmetry adapted basis set based on the $\mathcal{D}_{nh}$ symmetry point group is used. As an illustration of the $3N-5$ model presented, TROVE has been used to compute an *ab initio* room temperature line list for $^{12}C_2H_2$ using symmetry-adapted *ab initio* potential energy (CCSD(T)-F12c/cc-pVQZ-F12) and dipole moment surfaces for the ground electronic state. Line positions and intensities ($J \leq 58$, $l < 8$, covering the wavenumbers up to 10 000 cm^{-1}) are compared against HITRAN-2016 and ASD-1000. Alternative methods for treating linear molecules and future work are discussed. https://doi.org/10.1063/1.5031844

I. INTRODUCTION

The linear structure of acetylene, $^{12}C_2H_2$, a chain of two of the most ubiquitous atoms in the universe, has long been considered a special case in accurate ro-vibrational variational calculations. It has spectra of importance for modeling a host of interesting environments throughout the galaxy, necessitating spectral data to be appropriate for a range of temperatures. On Earth, this involves monitoring various systems such as acetylene in breath, giving insights into the nature of exhaled smoke,[1] the hot oxy-acetylene flames used for welding and related activities,[2] and air-born pollutants.[3,4] Further out in our solar system, acetylene is found in the atmospheres of cold gas giants, Saturn,[5] Uranus,[6] and Jupiter,[7,8] the hydrothermal plumes of Enceladus,[9] and in the remarkably early-earth-like atmosphere of Titan.[10,11] It has been detected on comets such as Hyakutake,[12] Halley, and 67P/Churyumov-Gerasimenko.[13] Even further into the galactic neighbourhood, acetylene appears in star forming regions,[14] is speculated to be an important constituent of clouds in the upper atmospheres of brown dwarfs and exoplanets,[15–17] and is thought to play an important role in dust formation[18] and asymptotic giant branch (AGB) star evolution and atmospheric composition.[19–24]

Accurate and complete spectral data for $^{12}C_2H_2$ are a missing component in investigations into many of these situations, particularly those at high temperatures; its presence has been speculated in the atmosphere of hot super-earth 55 Cancri e[25] and carbon-rich stars in the Large Magellanic Cloud (LMC),[21,26,27] but more complete data than are currently available are required for accurate verifications in such high temperature environments. Alternative data were used: low-temperature data from HITRAN in the case of Ref. 21 and opacity sampling from Ref. 28 in the case of Refs. 26 and 27.

From a theoretical perspective, there have been a number of previous attempts to perform *ab initio* variational calculations on the ground electronic state of $^{12}C_2H_2$,[29–34] but these are apparently currently too computationally demanding to make them viable for calculations up to the highly rotationally excited states that have been calculated in this work, and only data for low ro-vibrational excitations are presented in the literature. Effective Hamiltonian and similar approaches have been implemented to obtain spectra up to a relatively high excitation.[19,35–37] However, while such approaches are stereotypically very good in the areas of the spectrum with many experimental data, they would not be expected to extrapolate so accurately up to higher energies and thus do not offer the coverage that variational calculations do. Comprehensive accurate opacities and cross sections, valid up to high temperatures, are therefore still desirable for many areas of astrophysics. Here we present a variational approach based on a mixture of *ab initio* and empirical models, which can be (and is in the process of being) used in high ro-vibrational energy calculations to produce such accurate high-temperature opacities and cross sections for $^{12}C_2H_2$.

Accurate laboratory data provide a vital component in the calculation of such spectra, for both effective Hamiltonian and the majority of variational approaches. Fortunately for $^{12}C_2H_2$, a wealth of experimental ro-vibrational spectral data has been recorded over the decades.[36–40] A recent collation and analysis of all available experimental data to date can be found in Ref. 41.

High quality variational spectra have been calculated up to high temperatures for a host of molecules, including CH_4,[42–44]

[a)]Electronic mail: katy.chubb.14@ucl.ac.uk
[b)]Electronic mail: s.yurchenko@ucl.ac.uk

HCN/HNC,[45] PH_3,[46] H_2O_2,[47] SO_2,[48] H_2S,[49] SO_3,[50] VO,[51] CO_2,[52] SiH_4,[53] NH_3,[54] H_2O,[55] and C_2H_4,[56] as part of the ExoMol project,[57,58] a database of highly accurate and comprehensive line lists, appropriate for modeling exoplanet, brown dwarf, or cool stellar atmospheres. Other extensive molecular spectroscopic databases include HITRAN,[59] HITEMP,[60] CDMS,[61] GEISA,[62] TheoReTS,[63] SPECTRA,[64] MeCaSDA, and ECaSDa.[65] Line lists for C_2H_2 can be found in HITRAN as well as in Refs. 35 and 37. The former is incomplete, while the latter are based on the theory of effective Hamiltonians, which, although accurate in the regions of many experimental data, tend to extrapolate poorly for high vibrationally excited states for which no experimental data are available.

A review of the software used to model molecules as part of the ExoMol project is given in Ref. 66: Duo[67] computes vibronic spectra for diatomics, DVR3D[68] computes rotation-vibration spectra for triatomics, and Theoretical ROVibrational Energies (TROVE)[69,70] computes rotation-vibration spectra for general polyatomic systems. All three programs are publicly available from https://github.com/ExoMol. This work focuses on TROVE and the updates made to allow for linear polyatomic molecules.

It has previously been shown (see Sec. II for details) that some special consideration is required to handle the singularities which would occur if standard Hamiltonians and number of internal coordinates are used in ro-vibrational calculations of linear molecules. Two general options exist: (i) the so-called ($3N$–6)-approach, which involves using the same form of the kinetic energy operator (KEO) as in the non-linear case, while modifying the form of the wave function (more specifically, the basis set of functions used to represent the wave function of the system) and (ii) the so-called ($3N$–5)-approach, according to which the form of the kinetic energy operator (KEO) is modified by treating one of the rotations as part of the internal "vibrational" modes, making $3N$–5 in total (where N is the number of atoms).

In the first ($3N$–6) approach, it is necessary to carefully choose the form of the basis functions to ensure that when the wave function is acted on by the singular KEO of the system it cancels the singularity. A popular choice which is used in WAVR4,[71] DVR3D,[68] and many other studies[29,72–83] is the use of angular basis functions which include Legendre polynomials, such as spherical harmonics. An alternative form of the wave function for linear triatomic molecules was developed in Refs. 84 and 85, which is not restricted to the use of spherical polar coordinates. This idea was originally formulated for triatomics but has been extended in this work for tetratomic molecules; see Sec. IV.

WAVR4 is an example of a computational method for ro-vibrational calculations capable of treating linear four-atomic molecules within the $3N$–6 approach[71,86] which uses the finite basis representation (FBR) for the angular coordinates and a mixed FBR-DVR basis for the radial motion. While accurate at low excitations of rotational energy, it is currently too computationally demanding to make it viable for use up to highly rotationally excited states.[34,87] WAVR4 was used to calculate the ro-vibrational energy levels and spectra of acetylene, up to rotational excitation $J = 1$[34,71] (with extrapolations to higher rotational excitations[34]). As stated in the papers, the program was specifically designed to deal with wide amplitude motion and isomerizations; the isomerization from acetylene to vinylidene is expected to occur at around 15 000 cm^{-1} above the acetylene ground state.[31] DVR3D is a code used by the ExoMol project which utilises the DVR (Discrete Variable Representation) method, based on the Gauss-Jacobi and Gauss-Laguerre quadrature,[66,68] in the modeling of the ro-vibrational spectra of triatomic molecules and is capable of successfully handling linear molecules such as CO_2.[52,88]

The second ($3N$–5) approach involves choosing appropriate coordinates to represent a linear molecule which do not lead to singular terms in the KEO. One of the best known examples of such a $3N$–5 ro-vibrational Hamiltonian was published by Watson in 1968,[89] which uses normal coordinates and is still an important basis for a large amount of related work until the present day.[90–94] Its foundation is found in techniques developed in Ref. 95 for treating linear triatomic molecules in a doublet-Π electronic state and the work in Refs. 96, 97, and 95, in which the Hamiltonian is built in the classical form and transformed to the corresponding quantum operator form via the Podolsky trick[98] and employing the Eckart conditions.[99] An alternative form of the Hamiltonian, appropriate for linear molecules, was subsequently published by Watson,[100] which deals with the angular momentum around the linear axis differently to the standard non-linear case. There are similarities here with the method we employ in Sec. III; the Euler angle describing rotation about the z-axis, i.e., χ (see Fig. 1), becomes undefined for a linear molecule, and so this rotational motion is effectively treated as vibrational instead.

The paper is structured as follows. Section II outlines the details of the traditional TROVE program procedure and why amendments are needed for linear molecules. Section III introduces the new ($3N$–5) approach to deal with linear molecules in TROVE. The potential energy and dipole moment surfaces

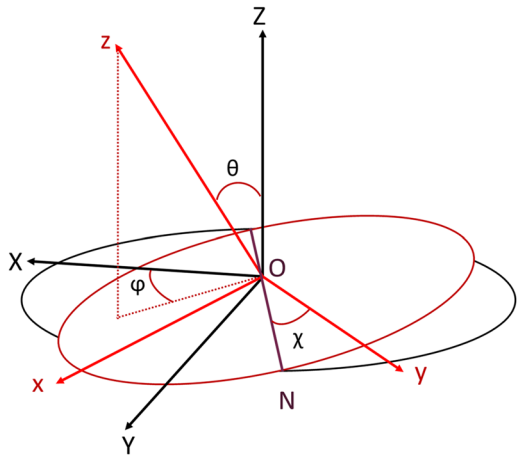

FIG. 1. The Euler angles describing the orientation of the molecular (x, y, z) axis (red) from the laboratory (X, Y, Z) axis (black). Here, θ is the angle between the Z and z axes, ϕ is the angle from X to the projection of z on the X–Y plane, and χ is the angle between from ON (purple) to the y-axis, where O is the origin of both axes and ON defines the node line, which is the intersection of the X–Y and the x–y planes. ON is also perpendicular to both the z and Z axes. χ is therefore the azimuthal angle about the z-axis.

used in calculations using this approach are given in Sec. V. Section IV outlines the (3N–6) approach for four-atomic linear molecules. Section VI presents the results of a room temperature line list for $^{12}C_2H_2$ using the (3N–5) approach and the *ab initio* surfaces presented in Secs. III and V, which is fully implemented into TROVE. Finally, Sec. VII offers our conclusions and some discussions of associated advantages and disadvantages of the approaches presented. The supplementary material is included, where the *ab initio* potential energy and dipole moment functions are given as Fortran subroutines, as described in Sec. VIII.

II. RO-VIBRATIONAL CALCULATIONS USING TROVE AND THE CONSTRUCTION OF THE KINETIC ENERGY OPERATOR

In order to fully understand why a special treatment is required for variational calculations involving linear molecules, it is necessary to look at the method used to solve for the ro-vibrational energies of non-linear molecules. Here we consider specifically the variational method TROVE; however, the conclusions are general enough to be applicable to other nuclear motion programs.

The ro-vibrational energies $E^{\rm rv}$ and wave functions $\Psi^{\rm rv}$ are obtained as a solution of the Schrödinger equation within the Born-Oppenheimer (B-O) approximation,

$$\hat{H}^{\rm rv}\Psi^{\rm rv} = E^{\rm rv}\Psi^{\rm rv}, \tag{1}$$

where $\hat{H}^{\rm rv}$ is the ro-vibrational Hamiltonian operator of the molecular system. Solving this variationally can be highly computationally demanding, especially for polyatomic molecules, with a general increase in time for systems with more atoms. With the B-O approximation comes the concept of potential energy surfaces (PESs); the Schrödinger equation should be solved for the motions of the nuclei moving in the potential created by the electrons. This is formed by using electronic structure calculations to find the total energy of a given electronic state as a function of clamped nucleus geometry. The nuclear Hamiltonian operator $\hat{H}$ is a sum of the kinetic energy operator and potential energy function,

$$\hat{H} = \hat{T} + V. \tag{2}$$

In TROVE, these operators are expanded as a Taylor series around the minimum of the potential energy surface (i.e., the equilibrium geometry) or, alternatively, around a non-rigid configuration, in terms of a suitable set of internal coordinates, ξ_i. For example, in the case of the potential energy function,[69]

$$V(\boldsymbol{\xi}) = \sum_{i,j,k,\ldots} f_{ijk\ldots}\xi_1^i\xi_2^j\xi_3^k\cdots, \tag{3}$$

where $f_{ijk\ldots}$ are expansion coefficients. This is appropriate as long as only the region around one minimum of the system is being considered, as is the case for $^{12}C_2H_2$ (we do not consider the isomerization of acetylene here). Typically this expansion is truncated around the 6th or 8th order term. A more in-depth account of this can be found in Ref. 69 (see also Sec. V). From here, we will focus on the kinetic energy operator, $\hat{T}$, which is calculated numerically in TROVE, as this is where the differences between linear and non-linear molecules occur.

The minimum number of coordinates required to describe the motions of any general molecule is 3N, where N is the number of atoms in the system: for a non-linear molecule, this breaks down as 3 to describe the position of the center of mass of the molecule [which is also the center of the molecular frame with respect to the laboratory frame (Fig. 1)] and 3 to describe the orientation of this frame (typically Euler angles in conjunction with the Eckart conditions;[101] see Fig. 1), leaving $M = 3N-6$ variables to describe the internal vibrational motions of the molecule, i.e., the stretches, bends, and dihedrals (see, e.g., Fig. 2). For linear molecules, this is not necessarily the case, as will be seen below.

The form of the KEO used in TROVE,[69] $\hat{T}$, is given by

$$\hat{T} = \frac{1}{2}\sum_{\lambda,\mu=1}^{M+3}\hat{p}_\lambda^\dagger G_{\lambda\mu}(\boldsymbol{\xi})\hat{p}_\mu + U(\boldsymbol{\xi}), \tag{4}$$

in terms of vibrational coordinates, $\boldsymbol{\xi} = \{\xi_1\ldots\xi_M\}$, angular momentum operators of the form $\hat{p}_{\lambda=1\ldots M+3} = \{-i\hbar\partial/\partial\xi_1 \ldots -i\hbar\partial/\partial\xi_M, \hat{J}_x, \hat{J}_y, \hat{J}_z\}$ (the momenta operators conjugate to the internal coordinates, along with three, x, y, and z, components of the total angular momentum operator, $\hat{J}$), and the pseudopotential function, $U(\boldsymbol{\xi})$. M is the number of internal (vibrational) degrees of freedom, typically 3N–6 = 6 for non-linear molecules.

$G_{\lambda\mu}(\boldsymbol{\xi})$ is a kinetic factor which we call the kinetic energy **G**-matrix, typically of dimensions M + 3, corresponding to the total number of ro-vibrational degrees of freedom. There is coupling between the rotational and vibrational motion, but the translational motion is always separable and so can be removed from these calculations. If this were not the case, then nuclear motion calculations would be unattainably difficult, as this translational motion essentially leads to a continuous spectrum (see, e.g., Ref. 77).

Using the nomenclature of Sørensen,[102] each element of $G_{\lambda\mu}(\boldsymbol{\xi})$ is given by

$$G_{\lambda\mu}(\boldsymbol{\xi}) = \sum_{i=1}^{N}\frac{1}{m_i}\sum_{\alpha=x,y,z} s_{\lambda,i\alpha}s_{\mu,i\alpha}, \tag{5}$$

where $s_{\lambda,i\alpha}$ is the Jacobian **s**-matrix ($\lambda = 1\ldots M+3$), which can be found via inversion of another matrix, called the Jacobian **t**-matrix. This is defined in three parts, associated with the M vibrational, 3 rotational, and 3 translational coordinates. These are given, respectively, by[102]

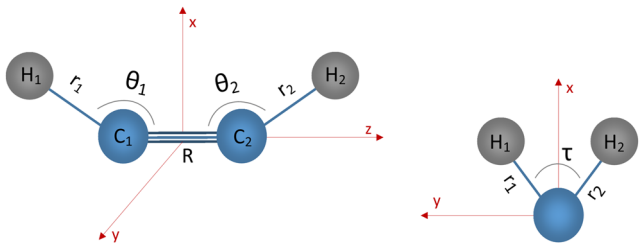

FIG. 2. HCCH as described using 3N–6 internal curvilinear coordinates.

$$t_{i\alpha,\lambda} = \frac{\partial r_{i\alpha}}{\partial \xi_\lambda} \quad (\lambda = 1 \ldots M+3), \tag{6}$$

$$t_{i\alpha,M+\beta} = \sum_{\gamma=x,y,z} \epsilon_{\alpha\beta\gamma} r_{i\gamma} \quad (\alpha, \beta = x, y, z), \tag{7}$$

$$t_{i\alpha,M+3+\beta} = \delta_{\alpha\beta} \quad (\alpha, \beta = x, y, z). \tag{8}$$

Here $r_{i\alpha}$ defines the Cartesian coordinates, $\alpha = x, y, z$, of each atom, $i = 1 \ldots N$, with respect to the center of mass of the system (body-fixed); ξ_λ is the λth vibrational coordinate and $\epsilon_{\alpha\beta\gamma}$ is the fully antisymmetric Levi-Civita tensor.

The **s**-matrix is defined by

$$s_{\kappa,i\alpha} = \frac{\partial \xi_\kappa}{\partial r_{i\alpha}}, \tag{9}$$

where ξ_κ is a generalised coordinate ($\kappa = 1, \ldots, 3N$) consisting of the translational, vibrational, and rotational coordinates. The **s**-matrix is related to the **t**-matrix by the chain rule

$$\sum_{i,\alpha} s_{k,i\alpha} t_{i\alpha,\mu} = \delta_{k\mu}. \tag{10}$$

In order to build the kinetic energy operator expansion, TROVE was originally programmed such that the **t**-matrix is first generated, before being numerically inverted as in Eq. (10) to obtain the rotational and vibrational elements of the **s**-matrix as expansions in terms of ξ_k, and in turn used to build the **G**-matrix expansions. However, improvements have been made since 2007[69] to reflect a method demonstrated by Sørensen[102] to reduce the size of matrices that are required to be inverted; these improvements will be outlined here.

Sørensen[102] makes use of a matrix of so-called "constraint vectors" $\boldsymbol{c}$, which in the Eckart embedding (as implemented in TROVE) are given by

$$c_{g,i\alpha} = m_i \sum_\beta \epsilon_{g\alpha\beta} r^{\mathrm{e}}_{i\beta}, \tag{11}$$

where $g = x, y, z$, $r^{\mathrm{e}}_{i\beta}$ is a β-Cartesian ($\beta = x, y, z$) component of the nucleus i at the equilibrium configuration, and $\epsilon_{g\alpha\beta}$ is the fully antisymmetric Levi-Civita tensor. These constraint vectors can be combined with the rotational **t**-vectors to form a new 3×3 matrix,

$$J_{gg'} = \sum_{i\alpha} c_{g,i\alpha} t_{g',i\alpha}, \tag{12}$$

which can be inverted to give $\eta_{gg'}$. That is, $\eta_{gg'}$ and $J_{gg'}$ are related as follows:

$$\sum_{g''} \eta_{g,g''} J_{g''g'} = \delta_{gg'}, \tag{13}$$

where $g, g' = x, y, z$. Once $\eta_{gg'}$ and $c_{g,i\alpha}$ have been found, they can be used to form the rotational part of the **s**-matrix,

$$s_{g,i\alpha} = \sum_{g'} \eta_{gg'} c_{g',i\alpha}. \tag{14}$$

Here, the $\eta_{gg'}$ coefficients are common to all atoms, reducing the number of elements required to be evaluated; only inversion of the 3×3 (4×4 for non-rigid representations[69,102]) **J**-matrix [Eq. (12)] is required. It is for this reason the method has been implemented in TROVE.

In the case of Eckart embedding, the **J**-matrix is linear in $r_{i\alpha}$.[102] We expand the $\boldsymbol{\eta}$-matrix as a Taylor series in terms of the vibrational coordinates ξ_λ,

$$\eta_{gg'} = \sum_{i,j,k,\ldots} \eta^{gg'}_{i,j,k,\ldots} \xi^i_1 \xi^j_2 \xi^k_3 \ldots \tag{15}$$

and solve iteratively for the coefficients by inverting the **J**-matrix of Eq. (12).

Once the rotational part of the **s**-matrix has been found in this way, the vibrational part can be found as follows.

TROVE's default choice is to use linearized internal coordinates describing the vibrational motion of the molecule. The **t**- and **s**-matrices are simplified by the linear transformation between Cartesian and linearized (rectilinear) coordinates $\xi^{\mathrm{lin}}_\lambda$,

$$r_{i\alpha} = r^{\mathrm{e}}_{i\alpha} + \sum_\lambda A_{i\alpha,\lambda} \xi^{\mathrm{lin}}_\lambda, \tag{16}$$

$$\xi^{\mathrm{lin}}_\lambda = \sum_{i,\alpha} B_{\lambda,i\alpha} (r_{i\alpha} - r^{\mathrm{e}}_{i\alpha}), \tag{17}$$

where $A_{i\alpha,\lambda}$ and $B_{\lambda,i\alpha}$ ($i = 1 \ldots N$, $\alpha = x, y, z$, $\lambda = 1 \ldots M$) are matrices of coefficients defining the direct and inverse transformation between the Cartesian and linearized coordinates. The linearized coordinates are obtained by linearization (Taylor expanding in terms of Cartesian displacements and truncating at the linear term) of the geometrically defined coordinates (GMD) such as bond lengths, inter-bond angles, and dihedral angles with respect to the Cartesian displacement from the equilibrium configuration.[101] The elements of the linearized $\boldsymbol{B}$-matrix are defined as the first derivatives of the Cartesian positions $r_{i\alpha}$ with respect to the GMD coordinates taken at the equilibrium and thus coincide with the vibrational elements of the **s**-matrix in Eq. (9) at the equilibrium,

$$B_{\lambda,i\alpha} = s^{\mathrm{e}}_{\lambda,i\alpha}. \tag{18}$$

The elements of the **A**-matrix are subject to the constraints of the center of mass, Eckart, and orthogonality conditions,

$$\sum_{i\alpha} B_{\lambda,i\alpha} A_{i\alpha,\lambda'} = \delta_{\lambda\lambda'}. \tag{19}$$

See Ref. 69 for details. In this case, the **J**-matrix in Eq. (12) becomes a simple linear function of $\xi^{\mathrm{lin}}_\lambda$. The vibrational part of **s** is also simplified. According to Sørensen,[102] it is now given by

$$s^{\mathrm{vib}}_{\lambda,i\alpha} = s^{\mathrm{e}}_{\lambda,i\alpha} - \sum_{g,\lambda'} \xi^{\mathrm{lin}}_{\lambda'} \zeta^g_{\lambda',\lambda} s^{\mathrm{rot}}_{g,i\alpha}, \tag{20}$$

which makes use of the rotational part of the **s**-matrix, $s^{\mathrm{rot}}_{g,i\alpha}$, and where $\zeta^g_{\lambda',\lambda}$ are the Coriolis coefficients

$$\zeta^g_{\lambda',\lambda} = \sum_{i\alpha\beta} \epsilon_{g,\alpha,\beta} A_{i\alpha,\lambda'} B_{\lambda,i\alpha}. \tag{21}$$

It can clearly be seen that if the determinant of the **t**-matrix which is used to build the KEO involves any bending angles it will tend to zero at linearity, and therefore inversion of this matrix in the process described above will lead to singular terms. For example, for the $3N$–6 coordinates illustrated in Fig. 2, the determinant of the **t**-matrix becomes zero at the linear geometry,

$$\det(\mathbf{t}) = 2\,\sin(\theta_1)\,\sin(\theta_2)\,R^2\,r_1^2\,r_2^2. \tag{22}$$

It should be noted that TROVE is now capable of working with geometrically defined coordinates as described in Ref. 70. Although the current description below is based on the linearized coordinates only, it is directly compatible with the methodology of Ref. 70.

III. TROVE AND THE SINGULARITY ISSUE: THE (3*N*–5) APPROACH

A. The coordinate system and KEO

As explored in Secs. I and II, the singularity issue in the KEO is associated with some of the angles used to describe the system becoming undefined at linearity. According to the (3*N*–5) approach, one of the rotational angles must be combined with the vibrational modes (the Euler angle describing the rotation of the molecule around the z axis, χ (see Fig. 1). Therefore, an extended set of the internal coordinates is defined to cover all vibrations as well as this rotation motion: (3*N*–5) coordinates. In the following, we show how this is now been implemented in TROVE to construct a (3*N*–5)-type kinetic energy operator (KEO) as part of TROVE's numerical "on-the-fly" methodology.

In the case of $^{12}C_2H_2$, the common choice of the 3*N*–6 curvilinear (geometrically defined) coordinates includes $R \equiv r_{CC}$, $r_1 \equiv r_{CH_1}$, $r_2 \equiv r_{CH_2}$, $\theta_1 \equiv \theta_{CCH_1}$, $\theta_2 \equiv \theta_{CCH_2}$, and $\tau \equiv \tau_{HCCH}$ (see Fig. 2). Thus, apart from the Euler angle χ (see Fig. 1), another "singular" coordinate is τ, describing the torsional motion of the molecule; τ is undefined if either of θs becomes 180°, while χ is undefined for the linear configuration $\theta_1 = \theta_2 = 180°$. Using any of these coordinates would introduce a singularity in the kinetic energy operator, even in the (3*N*–5) approach.

We define our singularity-free coordinates as follows. The equilibrium configuration $r^{\mathrm{e}}_{i\alpha}$ of a linear molecule is set along the molecular z-axis (centered at $z = 0$), as shown in Fig. 2. The positions of the H_1 and H_2 atoms are given by their (rectilinear) Cartesian x and y displacements relative to the equilibrium linear configuration (subject to the center of mass and Eckart conditions), supplemented by the bond length between the two carbon atoms R and the two carbon-hydrogen bonds lengths, r_1 and r_2. These seven coordinates ξ_λ [$\Delta x_1, \Delta y_1, \Delta r_1, \Delta x_2, \Delta y_2, \Delta r_2$, and ΔR, where $\Delta x_i = r_{i_x}$ and $\Delta y_i = r_{i_y}$ (i = 1, 2)] provide an (almost) unambiguous description of any instantaneous configurations of $^{12}C_2H_2$ including the linear geometry; such a choice, however, is not ideal to describe the vibrational motion of the molecule as the bond lengths r_1 and r_2 become ambiguous for the configurations with $\theta_i > 90°$ and $\theta_i < 90°$. As will be seen below, the linearized version of this set of coordinates does not have this problem.

Based on these seven coordinates ξ_λ, we also define seven linearized coordinates as follows. For the three stretching modes ξ_1^{lin}, ξ_2^{lin}, and ξ_3^{lin}, we use the linearized versions of the bond length displacements ΔR, Δr_1, and Δr_2. The linearization is defined by Taylor expanding them in terms of the Cartesian displacements Δx_i, Δy_i, and Δz_i (i = 1, 2, 3, 4) and truncating after the linear terms (see Sec. II).

The four rectilinear bending modes ξ_4^{lin}, ξ_5^{lin}, ξ_6^{lin}, and ξ_7^{lin} are defined as the Δx_i and Δy_i (i = 1, 2) Cartesian components of the hydrogen atoms H_1 and H_2 as follows:

$$\xi_4^{\mathrm{lin}} = \Delta x_1, \quad \xi_5^{\mathrm{lin}} = \Delta y_1, \tag{23}$$

$$\xi_6^{\mathrm{lin}} = \Delta x_2, \quad \xi_7^{\mathrm{lin}} = \Delta y_2. \tag{24}$$

See Refs. 82 and 103 for an alternative representation where the $\sin\theta_i$ projection on x_i and y_i is used. Technically, the x and y projections of the vectors CH_1 and CH_2 onto the molecular $\vec{e}_x$ and $\vec{e}_y$ axes are defined using the normals $\vec{n}_1$ and $\vec{n}_2$ to the CCH_1 and CCH_2 planes, respectively,

$$\begin{aligned} \Delta x_1 &= -(\vec{e}_y \cdot \vec{n}_1), \quad & \Delta y_1 &= (\vec{e}_x \cdot \vec{n}_1), \\ \Delta x_2 &= (\vec{e}_y \cdot \vec{n}_2), \quad & \Delta y_2 &= -(\vec{e}_x \cdot \vec{n}_2), \end{aligned} \tag{25}$$

where the normals $\vec{n}_i (i = 1, 2)$ are given by

$$\vec{n}_i = \frac{[\vec{R} \times \vec{r}_i]}{R\,r_i}. \tag{26}$$

See Fig. 3 for a description of these coordinates.

The molecular xyz-body fixed system is chosen according to the Eckart conditions[69] (see Fig. 1), and for this choice of coordinates, the coordinate transformation in Eq. (16) is given by

$$r_{i,x} = (A_{i,x,4}\,\xi_4^{\mathrm{lin}} + A_{i,x,6}\,\xi_6^{\mathrm{lin}}), \tag{27}$$

$$r_{i,y} = (A_{i,y,5}\,\xi_5^{\mathrm{lin}} + A_{i,y,7}\,\xi_7^{\mathrm{lin}}), \tag{28}$$

$$r_{i,z} = r^{\mathrm{e}}_{i,z} + (A_{i,z,1}\,\xi_1^{\mathrm{lin}} + A_{i,z,2}\,\xi_2^{\mathrm{lin}} + A_{i,z,3}\,\xi_3^{\mathrm{lin}}), \tag{29}$$

where the property $r^{\mathrm{e}}_{i,x} = r^{\mathrm{e}}_{i,y} = 0$ is taken into account. The matrix elements $A_{i\alpha,\lambda}$ [see Eq. (16)] are provided as part of the supplementary material. Thus, the rectilinear bending coordinates ξ_4^{lin}, ξ_6^{lin} and ξ_5^{lin}, ξ_7^{lin} are always directed along the x and y axes, respectively [see Eq. (25)], while ξ_1^{lin}, ξ_2^{lin}, and ξ_3^{lin} (i.e., ΔR^{lin}, $\Delta r_1^{\mathrm{lin}}$, and $\Delta r_2^{\mathrm{lin}}$) are along the z axis. Thus the stretching linearized coordinates ξ_2^{lin} and ξ_3^{lin} do not have the aforementioned ambiguous configuration when $\theta_i > 90°$ and $\theta_i < 90°$. They are, however, less physically intuitive as they do not support the chemical bonding between the atoms.

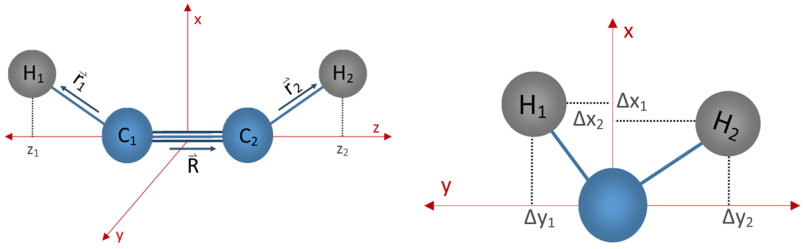

FIG. 3. HCCH as described using the 3*N*–5 coordinates employed in TROVE (see text). $\vec{R}$ is the vector (of length R) pointing from the first to the second carbon atom, C_1 to C_2, while $\vec{r}_i$ are the two CH_i bond vectors (of lengths r_i). The Δx_1, Δx_2, Δy_1, and Δy_2 notations of this diagram and Eq. (25) are to reflect the Cartesian projections of the CH_i bond vectors.

It is important to note that in this coordinate system the angular momentum defined by the remaining two Euler angles is conserved and thus all the standard commutation properties (with standard matrix elements of $\hat{\boldsymbol{J}}$) will still apply. This is not an obvious conclusion; see, for example, the discussion by Howard and Moss,[104] Sørensen,[102] or Watson,[105] who obtained different commutation relations for the corresponding $\hat{J}_x$, $\hat{J}_y$, and $\hat{J}_z$ components. However Hougen[95] and Howard and Moss[104] have shown that the normal commutation relations can be always restored via a suitable unitary transformation of the eigenfunctions. The consequence of this conclusion is that the standard procedure to build a KEO (e.g., based on the **s**- and **t**-matrices, as described in Sec. II) can be used with the only amendment being to remove the z-component, which thus causes the $\hat{J}_z$ terms to disappear in the KEO [Eq. (4)]. We apply the TROVE approach[69] to build the kinetic energy operator, where the z-components of all matrices (**t**, **s**, **G**) are set to zero. In other words, the angular momentum about the molecular axis is treated as purely vibrational, known as the Sayvetz condition for linear molecules.[105]

B. Basis set and its symmetrization

TROVE uses a general numerical symmetrization approach to build a symmetry adapted basis set, recently outlined in Ref. 106. It utilises the concept of a sum-of-product basis set, with one-dimensional (1D) vibrational basis functions $\phi_{v_i}(\xi_i)$ (where ξ_i is a generalised vibrational coordinate) and rigid-rotor (spherical harmonics) rotational basis functions $|J, k, m\rangle$, where J is the rotational angular momentum quantum number and k and m are the quantum numbers describing its projections on the molecular z and laboratory Z axes, respectively (with m commonly dropped or taken as $m = 0$),

$$\Phi^J_{k,v}(\theta, \phi, \chi, \xi_1, \xi_2 \ldots \xi_M) = |J, k, m\rangle\, \phi_{v_1}(\xi_1)\, \phi_{v_2}(\xi_2) \ldots \phi_{v_N}(\xi_M). \quad (30)$$

The 1D vibrational basis functions are either obtained by solving the corresponding reduced 1D Schrödinger equations or are taken as the Harmonic or Morse oscillators. Table I defines the TROVE local mode quantum numbers and shows how they correlate to the standard (normal mode) quantum numbers used to describe the rotational and vibrational states of $^{12}C_2H_2$. The latter are summarized in Table II.

For $^{12}C_2H_2$, we select the following three symmetry independent vibrational sub-spaces: (I) CC-stretch $\phi^{(1D)}_{v_1} = \phi_{v_1}(\xi^{\rm lin}_1)$; (II) CH-stretches $\phi^{(2D)}_{v_2 v_3} = \phi_{v_2}(\xi^{\rm lin}_2)\phi_{v_3}(\xi^{\rm lin}_3)$; (III) bends $\phi^{(4D)}_{v_4 v_5 v_6 v_7} = \phi_{v_4}(\xi^{\rm lin}_4)\phi_{v_5}(\xi^{\rm lin}_5)\phi_{v_6}(\xi^{\rm lin}_6)\phi_{v_7}(\xi^{\rm lin}_7)$.

The 1D basis functions from the subspaces (I) and (II) are generated by solving the corresponding reduced 1D Schrödinger equations, while the sub-space (III) is represented by identical 1D Harmonic oscillator functions [the harmonic constants $\tilde{\omega}_i$ are obtained from the corresponding second derivatives of $V(\boldsymbol{\xi})$ at the equilibrium geometry]. Each invariant sub-space is then processed through the corresponding reduced Schrödinger equation (1D, 2D, and 4D, respectively). The eigenfunctions obtained are classified according to the $\mathcal{D}_{n\rm h}$ point group symmetry (as opposed to the infinite-order $\mathcal{D}_{\infty\rm h}$ point group). See Ref. 107 for the full details of the $\mathcal{D}_{n\rm h}$-symmetrization approach. The symmetrized eigensolution of sub-space (III) leads to a solution of the 4D isotropic oscillator in the $\mathcal{D}_{\infty\rm h}$ representation.

In order to facilitate the symmetrization of the bending 4D basis set functions

$$\phi^{(4D)}_{v_4 v_5 v_6 v_7} = \phi_{v_4}(\xi^{\rm lin}_4)\, \phi_{v_5}(\xi^{\rm lin}_5)\, \phi_{v_6}(\xi^{\rm lin}_6)\, \phi_{v_7}(\xi^{\rm lin}_7),$$

these functions are first found as eigenfunctions of $\hat{L}^2_z$, where the vibrational angular momentum operator is given by

$$\hat{L}_z = \sum_{\lambda,\lambda'} \xi^{\rm lin}_\lambda \zeta^z_{\lambda,\lambda'} \hat{p}_{\lambda'}. \quad (31)$$

Here, $\hat{p}_\lambda$ is a vibrational momentum operator and $\zeta^z_{\lambda,\lambda'}$ are Coriolis coefficients[102] [see Eq. (21)]. This allows us to divide the basis set into independent sub-groups with different values of the vibrational angular momentum quantum numbers $L = |l|$. It also facilitates another important constraint for the $(3N-5)$ approach to linear molecules that the rotation and vibrational basis sets need to be coupled according to the angular momentum rule $K = L$ (see, for example, Refs. 100 and

TABLE I. Quantum numbers used to classify the energy states of $^{12}C_2H_2$ in TROVE. See Table II for the description of the standard, normal mode quantum numbers n_1, n_2, n_3, n_4, l_4, and l_5.

TROVE	Description
v_1	CC-stretch (1D), $v_1 = n_2$
v_2, v_3	CH-stretches (2D), $v_2 + v_3 = n_1 + n_3$
v_4, v_5, v_6, v_7	Bends (4D), $v_4 + v_5 + v_6 + v_7 = n_4 + n_5$
L	Total vibrational angular momentum, $L = \lvert\ell_4 + \ell_5\rvert$
$K = \lvert k\rvert$	Rotational quantum number; z-projection of the rotational angular momentum
J	Quantum number associated with rotational angular momentum, **J**
$\Gamma_{\rm vib}$	Vibrational symmetry
$\Gamma_{\rm rot}$	Rotational symmetry
Γ	Total symmetry, $\Gamma_{\rm vib} \otimes \Gamma_{\rm rot}$, can be related to *e/f* and *ortho/para*

TABLE II. Standard quantum numbers used to classify the energy states of acetylene, $^{12}C_2H_2$. n_i ($i = 1\ldots5$) and L are normal mode quantum numbers. See Ref. 41 for further details.

Label	Description
n_1	CH symmetric stretch (σ^+_g)
n_2	CC symmetric stretch (σ^+_g)
n_3	CH antisymmetric stretch (σ^+_u)
n_4	Symmetric (trans) bend (π_g)
ℓ_4	Vibrational angular momentum associated with v_4
n_5	Antisymmetric (cis) bend (π_u)
ℓ_5	Vibrational angular momentum associated with v_5
L	Total vibrational angular momentum, $\lvert\ell_4 + \ell_5\rvert$
$K = \lvert k\rvert$	Rotational quantum number; z-projection of the rotational quantum number, J
J	Quantum number associated with rotational angular momentum, **J**
e/f	Symmetry relative to the Wang transformation (rotational state parity)
Ortho/para	Nuclear spin state

108), where $K = |k|$, which requires the states to be classified by L.

The vibrational basis set is then processed through a double-layered contraction scheme,[106] where (i) symmetrically independent modes are combined and used to solve reduced Hamiltonian problems resulting in symmetrized combinations of the corresponding basis functions and (ii) then used to solve the vibrational ($J = 0$) problem. The final contracted TROVE basis functions are given by symmetrized products of the rotational and vibrational basis functions,

$$\Phi^{J,\Gamma}_{v,L,K} = \Phi^{\Gamma_{\rm vib}}_{v,l} \otimes |J, K, \Gamma_{\rm rot}\rangle, \tag{32}$$

where $\Phi^{\Gamma_{\rm vib}}_{v,l}$ is a vibrational ($J = 0$) eigenfunction of the pure vibrational Hamiltonian $\hat{H}_{\rm vib}$ which transforms according to the $\Gamma_{\rm vib}$ irreducible representation (irrep),[101] v is a generic vibrational quantum number, and l refers to the vibrational angular momentum quantum number, with $L = |l|$; $|J, K, \Gamma_{\rm rot}\rangle$ is a symmetrized linear combination of rotational basis functions which transform according to the $\Gamma_{\rm rot}$ irrep (usually $K = |k|$, $K = 0, 1, \ldots, J$), and Γ is one of the irreps of the direct product $\Gamma_{\rm vib} \otimes \Gamma_{\rm rot}$. The $(3N–5)$ treatment requires that the condition $K = L$ is fulfilled (see, for example, Refs. 100 and 108); otherwise nonphysical states would be included in the basis set and the solution. Details on the general symmetrization approach in TROVE can be found in Ref. 106, with updates for linear molecules in Ref. 107.

In the case of a linear molecule such as HCCH, both the vibrational $\Phi^{\Gamma_{\rm vib}}_{v,l}$ and rotational $|J, K, \Gamma_{\rm rot}\rangle$ basis functions must transform according to the infinite molecular point group $\mathcal{D}_{\infty h}$, while the total nuclear-rotation-vibration eigenfunction spans a four-dimensional irrep of the finite $\mathcal{D}_{\infty h}$ (M) molecular symmetry group or is isomorphic to it.[107] The latter constraint can be also interpreted within the irreps of the point group $\mathcal{D}_{\infty h}$ as follows. The $\mathcal{D}_{\infty h}$ point group spans the following irreps: $A_{1g}, A_{2g}, A_{1u}, A_{2u}, E_{1g}, E_{1u}, \ldots E_{k(g/u)}$ ($k = 1, 2, \ldots, \infty$). The rotational and vibrational basis symmetries $\Gamma_{\rm vib}$ and $\Gamma_{\rm rot}$ spanning these irreps can also be associated with the corresponding value of the projection of the angular momenta (vibrational L or rotational K) on the z axis: the A-type irreps are those with a zero value of L (or K), while the E_k irreps are characterised by the angular momentum quantum number k. Hence, both $\Phi^{\Gamma_{\rm vib}}_{v,l}$ and $|J, K, \Gamma_{\rm rot}\rangle$ can span any irreps with the corresponding value of the angular momentum, L or K, while the total nuclear-rotation-vibration function in Eq. (32) can span only the A-type irreps Γ of $\mathcal{D}_{\infty h}$ (see Ref. 107 for a full account of symmetry in the case of a $\mathcal{D}_{\infty h}$ linear molecule, including the TROVE symmetrization procedure).

Since TROVE can only work with finite symmetries, instead of $\mathcal{D}_{\infty h}$, we use a finite group $\mathcal{D}_{nh}$ with a value of n large enough to cover all required excitations (up to $L_{\rm max} = K_{\rm max}$) such that $n = 2L_{\rm max} + 1$ or $n = 2L_{\rm max} + 2$[107] (depending on whether n is odd or even); it should be noted that odd and even values of n lead to different symmetry operations, but both are valid. For example, in order to be able to cover the rotational excitation up to $K = 10$ (E_{10g} and E_{10u}), it is necessary to use at least the $\mathcal{D}_{21h}$ symmetry. Evidently, the higher the required maximum rotational excitation, represented by $K_{\rm max} = L_{\rm max}$, the higher the n needed, leading to an increase in calculation time and a larger number/greater size of files to be stored. The minimum value of n required for the correct treatment ($n = 2L + 1$ or $n = 2L + 2$) should therefore be used (see Ref. 107). The symmetry $\mathcal{D}_{nh}$ with an odd number n is perhaps better suited to represent the infinite group as the even groups contain the B_g and B_u irreps not present in $\mathcal{D}_{\infty h}$. However, these will disappear from calculations in either case, and the point group inversion i is present in $\mathcal{D}_{nh}$, whereas for n odd it is not.[107] Since $i \in \mathcal{D}_{\infty h}$, in some sense an even-$n$ $\mathcal{D}_{nh}$ is more similar to $\mathcal{D}_{\infty h}$ than an odd-n $\mathcal{D}_{nh}$. It could thus be argued that only even-n $\mathcal{D}_{nh}$ groups should be considered in the limit of $n \to \infty$; this is the approach that has been taken in this work and that of Ref. 107.

In fact, the vibrational angular momentum quantum number L (and thus also K) can effectively be truncated based on the energy criteria: since the vibrational angular momentum l of a multi-dimensional isotropic harmonic oscillator[101] is bounded by the total vibrational quantum number N, the corresponding energy is limited by $E_{\rm max} \sim \tilde{\omega} \times N$ ($\tilde{\omega}$ is a harmonic frequency). The rotational quantum number k is bounded by J, with the energy contribution proportional to a much smaller value ($\sim BJ(J + 1)$). In this work, we have truncated the vibrational basis set at $L_{\rm max} = 8$, which also limits K to $K_{\rm max} = 8$ and requires the use of at least $\mathcal{D}_{17h}$.

This reduction in the basis set size is an advantage for the calculation time of total ro-vibrational energies; indeed, while calculations for high values of J are usually a bottleneck in ro-vibrational calculations using TROVE, or similar variational routines, for linear TROVE this is not the case. Here, increasing the value for the vibrational angular momentum leads to more of a bottleneck, but once the $J = 0$ representation has been computed, it is not computationally demanding to go to high values of rotational excitation, J. See Ref. 54 for more details on the process of utilising the $J = 0$ representation in TROVE for making ro-vibrational calculations more tractable; this also facilitates the option to replace vibrational band centers with experimentally determined values.[41]

The model outlined in this section, along with the potential energy function given in Sec. V, was used in the calculation of the *ab initio* room temperature line list given in Sec. VI.

IV. TROVE AND THE SINGULARITY ISSUE: THE (3*N*–6) APPROACH

As mentioned in Sec. II, the KEO for a linear molecule in terms of $3N–6$ vibrational coordinates contains singularities that are manifested in the presence of negative exponents for coordinates describing bending vibrations. For acetylene, the torsion coordinate τ and that of overall k-type rotation around the molecule-fixed z-axis, χ, become indefinite upon the bending vibrational coordinates α_1 and α_2 approaching zero values, i.e., at the linear geometry of the molecule (see Figs. 1 and 2; note that α_1, α_2 are referred to in this section, which correspond to $\alpha_1 = \pi - \theta_1$ and $\alpha_2 = \pi - \theta_2$, with θ_1 and θ_2 given in the figures). Accordingly, parts of the KEO G-matrix (see Sec. II), describing vibrations with respect to the τ and χ coordinates and part of the pseudopotential term U, diverge as $1/\alpha_1^2$ or $1/\alpha_2^2$ at small values of the α_1 or α_2

bending coordinates. For example, the $1/\alpha_1^2$-divergent terms of the KEO for acetylene can be collected together into the expression

$$T^{(1)}_{\text{sing}} = \frac{1}{\sin^2\alpha_1}\left(-\frac{\hbar^2}{2}G^{(1)}_{\tau\tau}\frac{\partial^2}{\partial\tau^2} - \frac{i\hbar}{2}\left[G^{(1)}_{\tau\chi}+G^{(1)}_{\chi\tau}\right]\frac{\partial}{\partial\tau}\hat{J}_z + \frac{1}{2}G^{(1)}_{\chi\chi}\hat{J}_z^2 + U^{(1)}\right), \tag{33}$$

where the singular parts of the expressions for elements of vibrational $G^{(1)}_{\tau\tau}$, rotational $G^{(1)}_{\chi\chi}$ and Coriolis $G^{(1)}_{\tau\chi}$ and $G^{(1)}_{\chi\tau}$ matrices and pseudopotential $U^{(1)}$ are independent of α_1, α_2, and τ, and are functions of stretching coordinates only. In practical calculations, these are replaced by constant values computed at the equilibrium. An expression similar to Eq. (33) can be obtained for $T^{(2)}_{\text{sing}}$ by collecting terms in the total KEO with a $1/\sin^2\alpha_2$ factor. The explicit analytical expressions for $T^{(1)}_{\text{sing}}$ and $T^{(2)}_{\text{sing}}$ in the coordinate system defined as shown on Fig. 2 are not relevant for further discussion. We provide a script used for deriving the analytical KEO in the supplementary material.

We now require an appropriate form for the basis functions $\phi_1(\alpha_1)$ and $\phi_2(\alpha_2)$ that exactly cancels the divergence of the KEO in the vicinity of the linear geometry. From the pragmatic point of view of numerical calculations, the basis functions must be chosen such that they eliminate the singularity in the respective matrix elements. The most evident approach is to cancel the singularity in each term in (33) individually by using the forms $\phi_1(\alpha_1) \sim \alpha_1$ and $\phi_2(\alpha_2) \sim \alpha_2$. This is satisfied, for example, by choosing the Legendre orthogonal polynomials as a basis that approach zero at linearity. For this reason, Legendre based polynomials have been employed as suitable basis functions for solving the bending problem in many variational ro-vibrational approaches.[29,72–81]

Here, we follow the alternative approach developed in Refs. 101 and 109 for triatomic molecules, which attempts to find the exact form of the bending wave function in the vicinity of the linear geometry. It is based on the fact that since neither the energy nor the wave function can be singular, the Hamiltonian operator acting on a wave function has to produce a non-singular function as well. Therefore, the divergence of $T^{(1)}_{\text{sing}}$ and $T^{(2)}_{\text{sing}}$ must be exactly cancelled by other terms in the ro-vibrational Hamiltonian: the kinetic energy operators for the α_1 and α_2 vibrations. This can only be so if the wave function $\phi_{v_1}(\alpha_1)$ satisfies the equation

$$-\frac{\hbar^2}{2}G_{\alpha_1\alpha_1}\frac{\partial^2\phi_{v_1}(\alpha_1)}{\partial\alpha_1^2} + T^{(1)}_{\text{sing}}\phi_{v_1}(\alpha_1) = 0 \quad \text{at } \alpha_1 = 0, \tag{34}$$

with a similar expression for $\phi_{v_2}(\alpha_2)$. If we choose the basis functions for χ and τ coordinates to be $\phi_k(\chi) = (2\pi)^{-1/2}e^{ik\chi}$ and $\phi_t(\tau) = (2\pi)^{-1/2}e^{it\tau}$ (k and t are quantum numbers associated with χ and τ, respectively), the integration of (34) over the χ and τ variables yields

$$G_{\alpha_1\alpha_1}\frac{\partial^2\phi_{v_1}(\alpha_1)}{\partial\alpha_1^2} - \frac{1}{\sin^2\alpha_1}\left(t^2G^{(1)}_{\tau\tau} + kt\left[G^{(1)}_{\tau\chi}+G^{(1)}_{\chi\tau}\right] + k^2G^{(1)}_{\chi\chi} + \frac{2}{\hbar^2}U^{(1)}\right)\phi_{v_1}(\alpha_1) = 0. \tag{35}$$

The solution of this equation implies that for small α_1 the wave function behaves as

$$\psi_{v_1}(\alpha_1) \sim (1-\cos^2\alpha_1)^{1/4}L^{m_1}_{n_1}(\cos\alpha_1), \tag{36}$$

where $L^{m_1}_{n_1}(\cos\alpha_1)$ is the associated Legendre function of the first kind, a solution to the associated Legendre differential equation[110] with

$$n_1 = -\frac{1}{2}, \tag{37}$$

$$m_1(k,t) = \sqrt{\frac{1}{4} + \frac{t^2G^{(1)}_{\tau\tau} + kt\left[G^{(1)}_{\tau\chi}+G^{(1)}_{\chi\tau}\right] + k^2G^{(1)}_{\chi\chi} + 2U^{(1)}/\hbar^2}{G_{\alpha_1\alpha_1}}}. \tag{38}$$

Similar expressions can be obtained for $\psi_{v_2}(\alpha_2)$. At small values of the argument α_1, the wave function in (36) can be reduced to the expression

$$\psi_{v_1}(\alpha_1) \sim \alpha_1^{\frac{1}{2}\pm m_1(k,t)}, \tag{39}$$

where plus and minus signs indicate two solutions for α_1 varying in the positive $[0, \pi]$ and the negative $[0, -\pi]$ directions, respectively. From Eq. (39), it follows that bending basis functions are intrinsically coupled with the torsional and k-type rotational molecular motions through parametric dependence

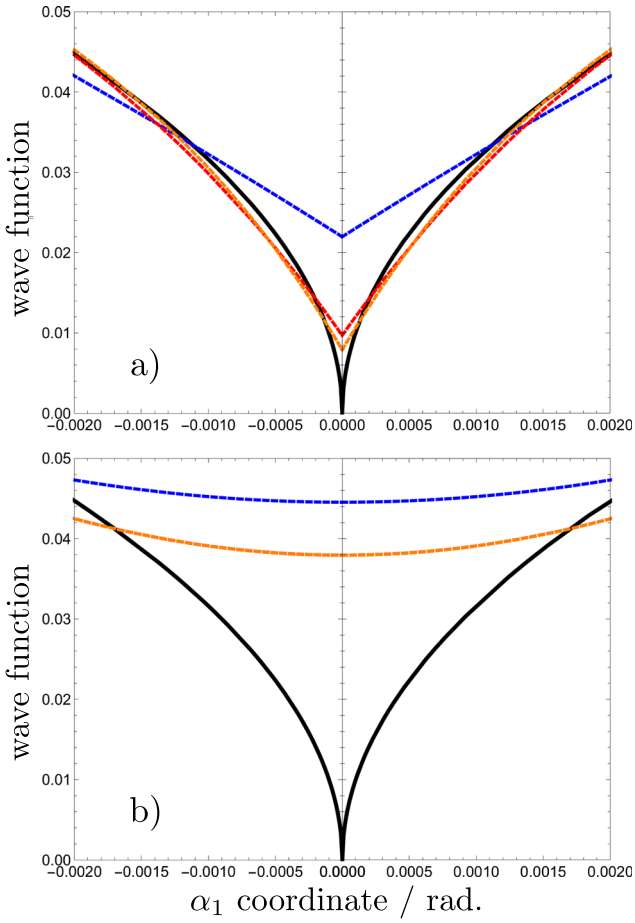

FIG. 4. Comparison of the exact bending wave function given by Eq. (39) with k, $t = 0$ (black line in both panels), with least squares fits of standard Legendre polynomial series truncated at $n_{\max} = 2$ (blue), 6 (red), and 10 (orange), for $L_n(\alpha)$ [panel (a)] and $L_n(\cos\alpha)$ [panel (b)]. The fit was done on an equidistant grid of α_1 values from $\alpha_1 = 0°$ to 1°.

on the respective quantum numbers k and t. More importantly, the bending wave function of a linear molecule behaves as a square root function and forms a non-differentiable cusp at the linear geometry (Fig. 4). The linearity-cusp in the wave function is not well reproduced by the commonly used expansions in terms of Legendre polynomials, as can be seen in Fig. 4. For the Legendre functions at the linear geometry ($\alpha = 0$), there is no cusp as the first derivative is constant and the convergence to the exact minimum point of the cusp is very slow. It is of interest to note the recent work of Hirano *et al.*,[111,112] who also come to the conclusion that the form of the bending wave function of a linear molecule has zero amplitude at $\rho = 0$, as in Fig. 4.

Work is in progress to implement the approach outlined in this section into TROVE. The presently implemented automatic numerical approach for building the power series expansion of the KEO is not capable of treating terms with negative exponents, which is the main obstacle to generalize the present method. For grid-based approaches, however, the implementation of the present method should be straightforward. Currently, the KEO is built externally using symbolic algebra packages and read in to TROVE.

It is thought that this approach could be applied to any chain tetratomic molecule and easily be extended to polyatomic molecules with more than four atoms. It will be interesting to test it also on chain molecules with a relatively high barrier to linearity, e.g., H_2O_2,[47,113] to see if the exact cusp conditions in Eq. (39) will be relevant for the basis set convergence of the variational results.

V. POTENTIAL ENERGY AND DIPOLE MOMENT SURFACES

Potential energy surfaces for acetylene are generally either local, appropriate for describing ro-vibrational motion close to the linear equilibrium structure,[103,114–117] or they are designed to be more global[33,78,118,119] in order to properly describe the isomerization to vinylidene at around 15 000 cm^{-1}.[31,120] The set of coordinates used to describe the potential are to some extent determined by this choice; curvilinear coordinates have been thought to represent a non-isomerising potential energy surface (PES) more smoothly than rectilinear,[120,121] though the difference is small in the region very close to equilibrium geometry; while coordinates such as diatom-diatom are thought to handle the isomerization process more appropriately.[29]

The use of a Taylor series expansion in an appropriate set of coordinates to represent the potential can only be justified for the local surfaces, restricted to accurately describe the area around one potential minimum only at which the expansion is taken: a linear configuration in this case. This is the approach which has been taken in this work (we do not consider the isomerization to vinylidene here). These are often truncated at fourth, sixth, or eighth order.

A. Potential energy functions: Linearized (3*N*–5) coordinates

In the TROVE rigid approach, all components of the Hamiltonian operator are represented as a Taylor expansion in terms of linearized coordinates (or some 1D functions of them) around the equilibrium configuration, leading to a sum-of-product form designed to facilitate the matrix element calculations via 1D-integrals. This includes the potential energy function $V(\boldsymbol{\xi})$. Since the PES is usually provided in terms of some different user-chosen curvilinear coordinates of a user-choice, TROVE uses a numerical finite difference method (with quadruple-precision) to re-expand $V(\boldsymbol{\xi})$ in terms of the TROVE-coordinates ξ_λ^{lin}.

The geometrically defined coordinates $\boldsymbol{\xi}$ (R, r_1, r_2, θ_1, θ_2, and τ) used to sample the *ab initio* PES were transformed to the linearized TROVE coordinates ξ_λ^{lin} using the Cartesian coordinate representation as an intermediate via the chain,

$$\boldsymbol{\xi} \rightarrow \{\boldsymbol{r}_i\} \rightarrow \boldsymbol{\xi}^{\text{lin}}, \tag{40}$$

with the transformation from $\boldsymbol{\xi}^{\text{lin}} \rightarrow \{\boldsymbol{r}_i\}$ given by Eqs. (27)–(29) via the **A**-matrix representation. Here $\{\boldsymbol{r}_i\}$ represents the Cartesian coordinates of an atom i in the molecular coordinate system defined using the Eckart-frame. This transformation is under-defined since there are only six coordinates ξ_λ being used to obtain seven ξ_μ^{lin}. As an additional condition, we use the requirement that the x-axis should bisect the dihedral τ angle. Since the potential expansion is built to be invariant for any rotation around the z axis, this requirement does not affect the expansion parameters.

For $^{12}C_2H_2$, we found that this numerical re-expansion procedure can behave very unstably, leading to extremely large expansion parameters and numerical instability. This is apparently related to the fact that if the $^{12}C_2H_2$ potential function is represented in the original *ab initio* coordinates, it effectively depends on six (3N–6) vibrational coordinates only, but we are representing it in terms of seven (3N–5) dependent coordinates. The expansion parameters are therefore strongly correlated, which leads to a numerical instability in the finite differences.

We therefore decided to avoid the TROVE re-expansion by preparing the PES in terms of the TROVE linearized coordinates $\boldsymbol{\xi}^{\text{lin}}$ directly (see Sec. III A). Thus, our potential energy function of $^{12}C_2H_2$ is given by

$$V(\boldsymbol{\chi}) = \sum_{i,j,k,\ldots} f_{i,j,k,\ldots} \chi_1^i \chi_2^j \chi_3^k \cdots, \tag{41}$$

where χ_λ are given by

$$\begin{aligned}
\chi_1 &= 1 - \exp\left(-a\,\Delta R^{\text{lin}}\right),\\
\chi_2 &= 1 - \exp\left(-b\,\Delta r_1^{\text{lin}}\right),\\
\chi_3 &= 1 - \exp\left(-b\,\Delta r_2^{\text{lin}}\right),\\
\chi_4 &= \Delta x_1,\\
\chi_5 &= \Delta y_1,\\
\chi_6 &= \Delta x_2,\\
\chi_7 &= \Delta y_2.
\end{aligned} \tag{42}$$

Here a and b are two Morse parameters and the displacements are taken from the equilibrium values of R, r_1, and r_2, respectively. The equilibrium values (at the linear configuration) of x_i and y_i are zero.

As discussed in Sec. III, the ground electronic state of acetylene has an equilibrium structure of linear configuration. The potential energy must therefore be invariant under the action of operations which span the $\mathcal{D}_{\infty h}$ point group,[107] e.g., to any rotation C_n around the z axis. As we tend to use discrete symmetries (see Sec. III), this is achieved by making it invariant to the operations of $\mathcal{D}_{nh}$ instead. While the process of symmetrizing the ro-vibrational basis set requires $\mathcal{D}_{nh}$ with a value for n such that $n \geq 2L_{max} + 1$ (odd n) or $n \geq 2L_{max} + 2$ (even n),[107] the same constraint does not need to be applied to the symmetrization of parameters to be used in the potential energy or dipole moment fitting routines. Instead, the required n for $\mathcal{D}_{nh}$ appears to be related to the expansion order of the potential; for a potential expanded up to 8th order, for example, a symmetry of $\mathcal{D}_{12h}$ is sufficient, with identical results for higher values of n. We therefore used the operations of the $\mathcal{D}_{12h}$ group to form our symmetrized $3N$–5 potential energy function, expanded up to 8th order.

The *ab initio* electronic structure calculations used in this work were performed using MOLPRO[122] at a CCSD(T)-F12c level of theory[123] with a VQZ-F12 basis set.[124] They were carried out on a grid of 50 000 points spanning the 6D nuclear-geometry coordinate space up to 15 000 cm^{-1}, defined by a set of 6 curvilinear bond length and bond angle coordinates (as given in Fig. 2).

When fitting $V(\boldsymbol{\xi})$ in Eqs. (41) and (42) to the *ab initio* energies, each grid point i was weighted using the method outlined in Ref. 125, with a higher weight, w_i, given to points with lower energy,

$$w_i = \frac{s_i}{\tilde{E}_i^w}, \tag{43}$$

$$s_i = \frac{\{\tanh[-\alpha(V_i - V^{\text{top}})] + 1.002\,002\,002\}}{2.002\,002\,002}, \tag{44}$$

$$\tilde{E}_i^w = \max(V_{\text{max}}, V_i). \tag{45}$$

Here, V_i is the potential energy, in cm^{-1}, above the equilibrium value for each point i, α is a parameter which can be varied, V^{top} is the "switching energy," with s_i switching between 0.001 for energies much above V^{top} and 1 for those much below, and $\tilde{E}_i^w$ is included in order to avoid low energy noise being too much of an influence, giving a bias against points below V_{max}. In the case of the linearized ($3N$–5) *ab initio* potential energy fit, the following parameters were used: $\alpha = 6 \times 10^{-4}$ cm, V_{top} = 20 000 cm^{-1}, and V_{max} = 6000 cm^{-1}.

A least squares fitting routine was used to fit the coefficients $f_{i,j,k,\ldots}$ in Eq. (41) to the *ab initio* energies, using a grid of 46 986 *ab initio* points covering up to 14 000 cm^{-1}, weighted as in Eqs. (43)–(45), with a weighted root-mean-square (*rms*) error of 3.98 cm^{-1} and an un-weighted *rms* of 15.65 cm^{-1}, using 358 symmetrized parameters expanded up to 8th order.

The Born Oppenheimer Diagonal Correction (BODC) is usually neglected in the Born-Oppenheimer approximation. It has been shown that the worst case for the BODC, for H_2, gives a correction of 16 cm^{-1}, whereas for acetylene this is estimated to be less than 1 cm^{-1} (Refs. 126 and 127). This has not been taken into account in the present work, but for greater spectroscopic accuracy this and other higher order corrections[128] could be taken into account in the future.

Different coordinates were explored with which to represent the potential function. The ($3N$–5) fit was found to improve when bond lengths (R, r_1, and r_2) instead of linearized coordinates (R^{lin}, r_1^{lin}, and r_2^{lin}) were used for the stretching coordinates (with a weighted *rms* error of 0.69 cm^{-1} and an un-weighted *rms* of 7.40 cm^{-1} for the same grid of weighted *ab initio* points up to 14 000 cm^{-1}); see Fig. 5 for the residuals of both ($3N$–5) fits (using linearized and non-linearized coordinates) as a function of energy. As mentioned above, this choice has a degeneracy in the definition of an instantaneous geometry for the interbond angles $\theta_i < 90°$ and $>90°$. It should be noted that the $\theta_i > 90°$ geometries are found to occur at energies less than the isomerization to vinylidene at around 15 000 cm^{-1} (Refs. 120 and 31) and are therefore likely to be important for ro-vibrational calculations. The linearized-coordinate alternative does not have this degeneracy issue, though it does have the aforementioned problem with being less intuitive in modeling vibrational stretches. Nevertheless, the linearized-coordinate fit to the potential energy function of Eqs. (43)–(45) is reasonable and the use of a potential function which has been fit using linearized coordinates avoids any re-expansion, as these are exactly the coordinates which are used by TROVE. We provide this PES fit using the ($3N$–5) linearized coordinates as given in the supplementary material. While this potential function is suited for use with TROVE, it is not necessarily so useful for the community. We therefore also provide a version of the PES which uses the standard six curvilinear coordinates R, r_1, r_2, θ_1, θ_2, and τ, with the χ-expansion variables (see Sec. V B).

B. 3*N*–6 potential surface

A Fortran least squares fitting routine was used to fit the *ab initio* points described in Sec. V A to functions of a Morse-oscillator form, as shown below for the $3N$–6 set of internal valence coordinates (as illustrated in Fig. 2),

$$V(\boldsymbol{y}) = \sum_{i,j,k,\ldots} F_{i,j,k,\ldots} y_1^i y_2^j y_3^k \cdots, \tag{46}$$

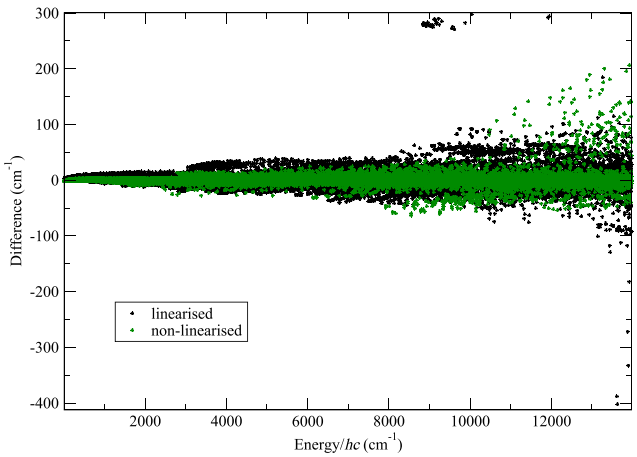

FIG. 5. A comparison of the residuals of the ($3N$–5) linearized coordinate fit with the ($3N$–5) non-linearized coordinate fit using the same grid of *ab initio* points.

where

$$\begin{aligned} y_1 &= 1 - e^{-a_1(R-R_e)}, \\ y_2 &= 1 - e^{-a_2(r_1-r_e)}, \\ y_3 &= 1 - e^{-a_2(r_2-r_e)}, \\ y_4 &= \sin(\theta_1), \\ y_5 &= \sin(\theta_2), \\ y_6 &= \cos(\tau). \end{aligned} \tag{47}$$

The use of Morse functions for the stretches has been shown to give a more accurate representation on the condition that the two atoms involved are suitably light,[29,129] as is the case for the bonds in the acetylene molecule. Care was taken to comply with the relevant symmetry constraints on the expansion coefficients $F_{i,j,k,\ldots}$, for example, if either of the bending angles were being expanded to the power of zero then the dihedral angle, τ should not be expanded to any power greater than zero, as for linear geometries it is undefined.

The same grid of 46 986 *ab initio* points is used as for the 3*N*–5 potential of Sec. V A, weighted as per Eqs. (43)–(45), with the same weighting parameters and equilibrium values used as in the (3*N*–5) fit. The (3*N*–6) fit, with the potential function expanded and truncated at 8th order, gives a weighted *rms* error of 1.30 cm^{-1} and an un-weighted *rms* error of 1.49 cm^{-1}, up to 14 000 cm^{-1} using 927 parameters. Again, the potential energy function is provided as part of the supplementary material as a Fortran program. As can be seen in Fig. 6, the residuals are smaller for the (3*N*–6) coordinate fit than for the fit using the (3*N*–5) linearized coordinates, with an increase as a function of *ab initio* energy, as would be expected as a result of the weighting of Eqs. (43)–(45). The better fit to the *ab initio* energies using the (3*N*–6) model is due to the curvilinear coordinates being chemically more intuitive to describe the internal stretching and bending motions of the molecule than the rectilinear type coordinates. As described previously (see Sec. V A), the re-expansion of this 3*N*–6 = 6 dimensional surface in terms of the set of 3*N*–5 = 7 coordinates used in TROVE is not currently stable, which is why this potential fit is not used in the calculations of Sec. VI, but it may be of use with other general nuclear motion routines, including the curvilinear version of TROVE; this version of the potential was used in testing the (3*N*–6) model outlined in Sec. IV.

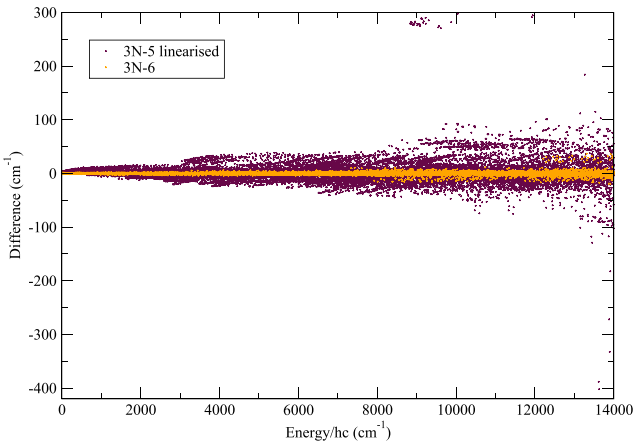

FIG. 6. A comparison of the residuals of the (3*N*–5) linearized coordinate fit of Sec. V A with the (3*N*–6) coordinate fit, both expanded up to 8th order and using the same equilibrium values and the same grid of *ab initio* points.

C. Dipole moment surfaces: (3*N*–5) coordinates

The *ab initio* electric dipole moment components, μ_α ($\alpha = x, y, z$), were computed using the finite difference method in MOLPRO, on a grid of 50 000 points spanning the 6D nuclear-geometry coordinate space covering up to 15 000 cm^{-1}, defined by a set of 3*N*–6 = 6 curvilinear bond length and bond angle coordinates (as given in Fig. 2), at the CCSD(T) level of theory and using an aug-cc-PVQZ basis set. The dipole moment surface was fit using the same set of 3*N*–5 coordinates as for the 3*N*–5 potential of Sec. V A (as illustrated in Fig. 3) to the following function:

$$\mu_x(\chi) = \sum_i F^x_{i,j,k,\ldots} \chi_1^i \chi_2^j \chi_3^k \ldots, \tag{48}$$

$$\mu_y(\chi) = \sum_i F^y_{i,j,k,\ldots} \chi_1^i \chi_2^j \chi_3^k \ldots, \tag{49}$$

$$\mu_z(\chi) = \sum_i F^z_{i,j,k,\ldots} \chi_1^i \chi_2^j \chi_3^k \ldots, \tag{50}$$

where χ_λ are given by

$$\begin{aligned} \chi_1 &= \Delta R^{\text{lin}}, \\ \chi_2 &= \Delta r_1^{\text{lin}}, \\ \chi_3 &= \Delta r_2^{\text{lin}}, \\ \chi_4 &= \Delta x_1, \\ \chi_5 &= \Delta y_1, \\ \chi_6 &= \Delta x_2, \\ \chi_7 &= \Delta y_2. \end{aligned} \tag{51}$$

Use was made of discrete symmetries (see Sec. III), and the three components of the dipole were expanded up to 7th order and symmetrized according to the operations of $\mathcal{D}_{12h}$ ($\mathcal{D}_{12h}$ is sufficient for the same reasons as the 3*N*–5 potential energy symmetrization of Sec. V A). The three Cartesian components of the dipole moment, μ_x, μ_y, μ_z, transform differently to one another [μ_x and μ_y as E_{1u} and μ_z as A_{2u} for $D_{nh}(M)$]:[101] the μ_x and μ_y components share the corresponding expansion parameters, while that the parameters for the μ_z component are independent.

Figure 7 gives the residuals of the dipole moment surface fit up to 14 000 cm^{-1} (for the *x*, *y*, and *z*-components of the dipole) using the (3*N*–5) linearized coordinates described in Sec. V A and illustrated in Fig. 3. The overall *rms* of the fit up to 14 000 cm^{-1} was 0.54×10^{-3} Debye [weighted with the same parameters as the potential energy fits, as per Eqs. (43)–(45)], and 0.75×10^{-3} Debye (unweighted), on a grid of 46 714 *ab initio* points, using 459 symmetrized parameters (259 and 200 for the *x*/*y* and *z* components, respectively). A version of the dipole moment function which is fitted in non-linearized coordinates is provided as part of the supplementary material as a Fortran program.

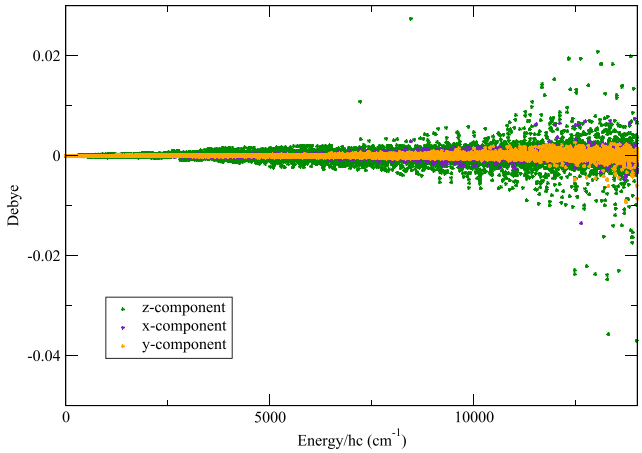

FIG. 7. Residuals of the dipole moment surface fit up to 14 000 cm^{-1} (for the x, y, and z-components of the dipole) using the set of ($3N$–5) linearized coordinates of Fig. 3.

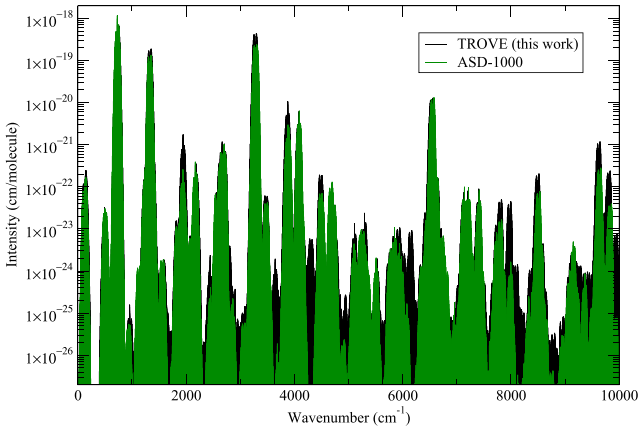

FIG. 8. Comparison of TROVE room-temperature *ab initio* spectrum (with linearized coordinates, up to 8th order expansion) with ASD-1000,[35] up to 10 000 cm^{-1} (TROVE calculations up to J = 58; transitions to higher J were not within the specified energy window of below 10 000 cm^{-1}).

VI. *AB INITIO* ROOM TEMPERATURE LINE LIST

A. Variational calculations

The ($3N$–5) model outlined in Sec. III has been fully implemented in TROVE. Here, we give an application to $^{12}C_2H_2$ in the form of an *ab initio* room temperature line list. The calculated *ab initio* potential energy and dipole moment surfaces used for this are presented in Secs. V A and V C.

The size of the primitive and contracted basis sets in Eq. (30) was controlled by the polyad number

$$P = v_1 + v_2 + v_3 + v_4 + v_5 + v_6 + v_7 \leq P_{\max}, \tag{52}$$

with $P_{\max}$ = 18 for the primitive basis set and reduced to 16 after contraction. Here, v_1 corresponds to the excitation of the C—C stretching mode, v_2 and v_3 represent the C—H_1 and C—H_2 stretching modes, and v_4, v_5, v_6, and v_7 represent the bending modes. The stretching primitive basis functions $\phi_{v_1}(\xi_1)$, $\phi_{v_2}(\xi_2)$, and $\phi_{v_3}(\xi_3)$ are generated using the Numerov-Cooley approach[69,130,131] as eigenfunctions of the corresponding 1D reduced stretching Hamiltonian operators $\hat{H}_i^{(1D)}$, obtained by freezing all other degrees of freedom at their equilibrium values in the J = 0 Hamiltonian. For the bending basis functions, $\phi_{v_4}(\xi_4), \ldots, \phi_{v_7}(\xi_7)$, 1D Harmonic oscillators are used. These basis sets are then divided into three sub-groups,

$$\phi_{v_1}^{(1D)}(\xi_1) = \phi_{v_1}(\xi_1), \tag{53}$$

$$\phi_{v_2 v_3}^{(2D)}(\xi_2, \xi_3) = \phi_{v_2}(\xi_2)\phi_{v_3}(\xi_3), \tag{54}$$

$$\phi_{v_4 v_5 v_6 v_7}^{(4D)}(\xi_4, \xi_5, \xi_6, \xi_7) = \phi_{v_4}(\xi_4)\phi_{v_5}(\xi_5)\phi_{v_6}(\xi_6)\phi_{v_7}(\xi_7). \tag{55}$$

The corresponding eigenvalue problems are solved for the three reduced Hamiltonian operators using these basis sets: stretching $\hat{H}^{(1D)}$ and $\hat{H}^{(2D)}$ and bending $\hat{H}^{(4D)}$. The reduced Hamiltonians $\hat{H}^{(ND)}$ (N = 1, 2, 4) are constructed by averaging the total vibrational Hamiltonian operator $\hat{H}^{(J=0)}$ over the other ground vibrational basis functions; see Ref. 107.

Energy cutoffs of 50 000 cm^{-1} and 30 000 cm^{-1} were set for the primitive and contracted matrices (see Sec. III), respectively, while the overall energy cutoff was set to 18 000 cm^{-1}. The D_{24h}(M) molecular symmetry group was used, which includes irreducible representations $A_{1g}, A_{2g}, B_{1g}, B_{2g}, A_{1u}, A_{2u}, B_{1u}, B_{2u}, E_{1g}, E_{1u}, E_{2g}, E_{2u}, \ldots, E_{11g}, E_{11u}$. As mentioned in Sec. III, only the A-type symmetry ro-vibrational states are allowed by nuclear statistics; the statistical weights are 1 for A_{1g} and A_{1u} (para), 3 for A_{2g} and A_{2u} (ortho), and 0 for everything else.[41,132] The kinetic energy and potential energy expansions are truncated at 2nd and 8th order, respectively (the kinetic energy terms of higher than 2nd order appear to contribute very little to the calculated ro-vibrational energies, with expansion to higher orders becoming more computationally demanding). The maximum value for the z-projection of the vibrational angular momentum, $K_{\max} = L_{\max}$, used to build the multidimensional basis sets was 8. The equilibrium bond lengths were set to 1.204 981 27 Å and 1.056 612 998 Å for the C–C and C–H bonds, respectively. Calculations were performed up to a maximum value of J = 58, with intensities calculated for transitions up to 10 000 cm^{-1} (transitions to higher J were not within this energy window), in order for a comparison to be made against a recent line list detailed below.

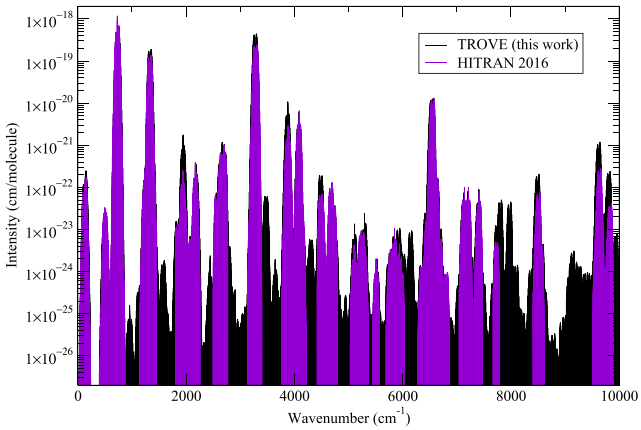

FIG. 9. Comparison of the TROVE room-temperature *ab initio* spectrum (using linearized coordinates, up to 8th order expansion) with the $^{12}C_2H_2$ data from HITRAN-2016,[59] up to 10 000 cm^{-1} (TROVE calculations up to J = 58; transitions to higher J were not within the specified energy window of below 10 000 cm^{-1}).

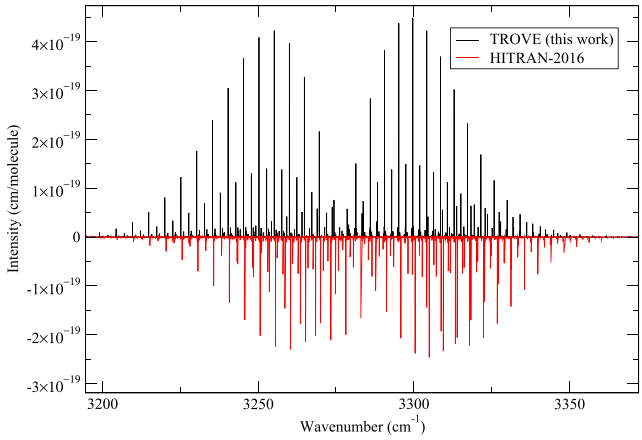

FIG. 10. Comparison of the ν_3 band from the TROVE room-temperature *ab initio* spectrum (using linearized coordinates, up to the 8th order expansion) with the same band using $^{12}C_2H_2$ data from HITRAN-2016.[59]

B. Comparison to other data

A recent line list, ASD-1000,[35] has been calculated by Lyulin and Perevalov up to 10 000 cm^{-1} and J = 100, based on the use of an effective Hamiltonian fit to experimental data and extrapolated to higher energies. The energies and intensities agree reasonably well with those in the HITRAN-2016[59] database (see Refs. 35 and 36 for detailed comparisons), and ASD-1000 has been used to update the 2016 HITRAN release in the low energy region.[59,133] Figure 8 gives a comparison of our *ab initio* line list with ASD-1000, and Fig. 9 shows a comparison of our work against the data for $^{12}C_2H_2$ in HITRAN-2016,[59] both at a temperature of 296 K. Figures 10 and 11 give more detailed comparisons of the fundamental ν_3 and ν_5 bands with data from HITRAN-2016.[59] No broadening coefficients or refinement of the *ab initio* potential energy surface to experimentally determined energies has been considered at this stage. Table III gives a comparison of the fundamental and some combination vibrational band centers of this work against the calculated energy term values $\tilde{E}^{\text{calc}}$ (cm^{-1}) presented in the study of Urru *et al.*[34] and experimental energy term values $\tilde{E}^{\text{obs}}$ (cm^{-1}) from Refs. 134, 41 and 34. Table IV gives a comparison of band intensities from this work with those presented in Ref. 135. There appears to be some inconsistencies in the labeling of bands between some of these data sources. For example, the ν_3 and $\nu_2 + (\nu_4 + \nu_5)$ bands are very close in energy and are both labeled as ν_3 in Ref. 135; care therefore needs to be taken when comparing values from different sources. For the sake of intensity comparisons, Vander Auwera *et al.*[136] have shown that the ν_3 and $\nu_2 + (\nu_4 + \nu_5)$ bands should be treated together, which results in a much larger intensity value for the ν_3 band than that reported in Ref. 135. Vander Auwera[137] also discusses the l-type resonance which couples the $(\nu_4 + \nu_5)^0$ and $(\nu_4 + \nu_5)^2$ bands.

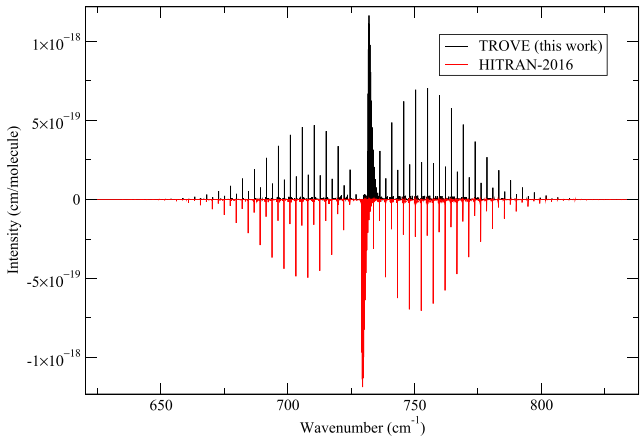

FIG. 11. Comparison of the ν_5 band from the TROVE room-temperature *ab initio* spectrum (using linearized coordinates, up to 8th order expansion) with the same band using $^{12}C_2H_2$ data from HITRAN-2016.[59]

TABLE III. Comparison of the fundamental and some combination vibrational band centers of this work against the calculated energy term values $\tilde{E}^{\text{calc}}$ (cm^{-1}) presented in the study of Urru *et al.*[34] and experimental energy term values $\tilde{E}^{\text{obs}}$ (cm^{-1}) from Refs. 134, 41 and 34. The obs.-calc. value given is the difference between $\tilde{E}^{\text{obs}}$ and $\tilde{E}^{\text{calc}}$ (cm^{-1}) (this work).

Band	Symmetry	$\tilde{E}^{\text{obs}}$	$\tilde{E}^{\text{calc}}$ (Ref. 34)	$\tilde{E}^{\text{calc}}$ (this work)	Obs.-calc.
ν_4^1	E_{1g}/Π_g	611.69[a]	602.9	610.55	1.14
ν_5^1	E_{1u}/Π_u	729.15[a]	722.2	732.78	–3.63
$2\nu_4^0$	A_{1g}/Σ_g^+	1230.39[b]	1203.5	1226.89	3.5
$(\nu_4+\nu_5)^0$	A_{2u}/Σ_u^+	1328.07[b]	1311.6	1330.73	–2.66
$2\nu_5^0$	A_{1g}/Σ_g^+	1449.11[b]	1448.6	1455.01	–5.9
ν_2^0	A_{1g}/Σ_g^+	1974.32[b]	1950.7	1974.47	–0.15
ν_3^0	A_{2u}/Σ_u^+	3294.84[b]	3241.1	3295.36	–0.52
ν_1^0	A_{1g}/Σ_g^+	3372.84[b]	3371.1	3365.04	7.8
$\nu_3+\nu_4^1$	E_{1u}/Π_u	3898.3[c]	3867.7	3899.69	–1.39

[a]Reference 134.
[b]Reference 41.
[c]Reference 34.

C. Discussion

A refinement procedure on the equilibrium bond-length geometry can vastly improve the accuracy of the rotational transitions but generally is balanced by a loss of accuracy on the vibrations.[139] In this work, we have adjusted the equilibrium bond-length geometry to give a good rotational structure, which may have negatively affected the vibrational band centers. Fortunately, there are other methods which can improve this, such as empirically refining the potential energy surface[140] or employing the empirical basis set correction (EBSC),[53] where the calculated vibrational band centers are replaced by their experimental values. We have not done either of these on the data presented in the current work but intend to refit the potential energy surface to a mixture of *ab initio* and experimentally determined energies; these semi-empirical adjustments are in progress for future publication, using the empirical energy levels of Ref. 41.

As expected, there is some obvious shifting of the band centers of our line list when compared to HITRAN-2016, as illustrated in Figs. 10 and 11, but the overall rotational structure is good. As can be seen in Table III, the ν_1 band gives the largest difference when compared to experimental data out of all the fundamental bands. The band intensities of Table IV are in general too high when compared to experimental values; $(2\nu_4 + \nu_5)^1$ II in particular stands out as having a very large percentage difference in the band intensity.

TABLE IV. Comparison of vibrational band intensities (S_{calc}) between this work and Ref. 135, along with S_{obs}, also from Ref. 135. Intensities were converted from cm^{-2} atm^{-1} to cm/molecule using the conversion of 1 cm^{-2} atm^{-1} at 296 K = 4.033×10^{-20} cm/molecule.[138] The observed values of the $(2\nu_4+\nu_5)^1$ I and $(2\nu_4+\nu_5)^1$ II bands are cited in Ref. 135, as from private communication with Di Lonardo. $\frac{O-C}{O}$ gives the relative $S_{obs} - S_{calc}/S_{obs}$ percentage difference between this work and the observed values presented in Ref. 135. The band centers ($\tilde{\nu}$) are in cm^{-1}.

Band	Symmetry	$\tilde{\nu}$ (Ref. 135)	$\tilde{\nu}$ (this work)	S_{calc}	S_{obs} (Ref. 135)	S_{calc} (this work)	$\frac{O-C}{O}$ (%)
ν_5^1	E_{1u}/Π_u	729.15[a]	732.85	2.3714×10^{-17}	2.3714×10^{-17}	2.3959×10^{-17}	−1.04
$(\nu_4+\nu_5)^0$	A_{2u}/Σ_u^+	1328.07[b]	1330.49	2.5408×10^{-18}	2.5408×10^{-18}	3.7799×10^{-18}	−48.77
$(2\nu_4+\nu_5)^1$ II	E_{1u}/Π_u	1941.2[c]	1945.12	5.6462×10^{-21}	5.6462×10^{-21}	3.7044×10^{-20}	−556.09
$(2\nu_4+\nu_5)^1$ I	E_{1u}/Π_u	1960.9[c]	1960.02	2.0165×10^{-21}	1.6132×10^{-21}	1.1662×10^{-22}	92.77
ν_3^0	A_{2u}/Σ_u^+	3294.84[b]	3295.19	4.2347×10^{-18}	4.3960×10^{-18}	9.0101×10^{-18}	−104.96

[a]Reference 134.
[b]Reference 41.
[c]Reference 135.

Some tests were done to compare the use of two different (3*N*–5) linearized-coordinate potential energy surfaces, each fit to the same set of *ab initio* energies and employing the same set of 3*N*–5 linearized coordinates, but each with a slightly different weighting scheme and parameters (see Sec. V A): we will label these as PES-1 and PES-2. The fit of PES-1 has a *rms* error of 123 cm^{-1} (unweighted) and 0.019 cm^{-1} (weighted), compared to 15.65 cm^{-1} (unweighted) and 3.98 cm^{-1} (weighted) for PES-2. A less computationally demanding small basis set [$P_{max} = 8$ for the primitive basis set and reduced to 6 after contraction, according to Eq. (52)] was used in order to make comparisons between the results of ro-vibrational calculations using PES-1 and PES-2. As expected, the energies shifted closer toward the corresponding experimental values for PES-2. There was, however, also an effect on the intensities (both calculations used the 3*N*–5 linearized coordinate DMS presented in Sec. V C), as illustrated by the $(\nu_4 + \nu_5)^0$ band in Fig. 12. It is apparent that the calculated intensities are very sensitive to the ro-vibrational eigenfunctions, which are dependent on the quality of the PES. We therefore expect the use of a potential energy surface with a better fit to lead to some improvement in both the energies of Table III and the intensities of Table IV; the procedure of refining the PES to empirical energies that is currently in progress is expected to improve the intensity values of Table IV, as is further experimenting with different weights in the DMS fitting procedure.

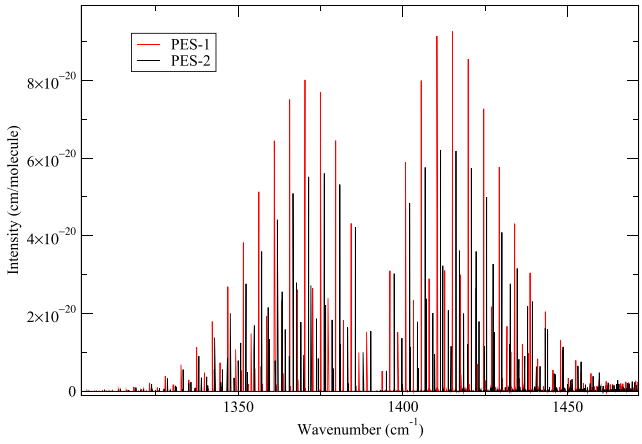

FIG. 12. An illustration of how different potential energy surfaces, with the same dipole moment surface, can have an effect on the intensities, in this case the $(\nu_4 + \nu_5)^0$ band (see Table IV). PES-1 and PES-2 were fit to the same 3*N*–5 function and *ab initio* points, as described in Sec. V A, but with different weighting parameters. A small basis set is used for testing purposes [$P_{max} = 8$ for the primitive basis set and reduced to 6 after contraction, according to Eq. (52)] due to the computational cost of high-basis-set calculations.

This is the focus of our current continuation of this work, for future publication: to further investigate the use of a different DMS, to include experimentally determined energies (of Ref. 41) in the potential energy surface fitting to give a semi-empirical PES, and to extend the calculations up to higher energies in order for it to be applicable up to high temperatures, of at least 1000 K.

VII. CONCLUSIONS

We have outlined two approaches to handle linear molecules in ro-vibrational calculations: 3*N*–5 and 3*N*–6. While the idea behind the (3*N*–6) approach is to select a form for the wave function which removes the singularity in the Hamiltonian, the (3*N*–5) approach makes use of a KEO which is already non-singular. The (3*N*–6) approach uses physically more meaningful and intuitive coordinates for representing the vibrations in the molecule; however, the main advantage of implementing the (3*N*–5) approach is that, unlike the (3*N*–6) approach or the use of Legendre Polynomial functions, it is compatible with the way that TROVE constructs and truncates basis sets to represent the full ro-vibrational wave function and still allows for the KEO to be generated numerically, with no analytical pre-derivation required (see Ref. 69 for more details). There is no reason why it should not be compatible with other polyatomic linear molecules, a supposition which will be put to test in the future. For these reasons, the (3*N*–5) approach has been fully implemented into TROVE along with a symmetrization procedure for linear molecules (details in Ref. 107) and was used in the calculations presented in Sec. VI. The (3*N*–6) approach will be integrated into TROVE in the future. The two approaches which make use of either 3*N*– 6 or 3*N*–5 internal coordinates should in principle lead to completely equivalent eigenvalues; a full comparison of these two approaches (calculation times, convergence, and

difference in accuracy) will be an interesting investigation to make.

We have shown that the ro-vibrational energy and intensity calculations using this (3*N*–5) model work with the variational method implemented in TROVE, with no numerical issues due to singularities in matrix elements, and that this method therefore has the potential, in combination with other techniques such as empirical PES refinement[140] or replacement of the band centers (EBSC),[53] to produce accurate high-temperature ro-vibrational spectra for $^{12}C_2H_2$. This has not been achieved before; previous variational calculations (such as in Refs. 29–34) did not provide coverage up to the high excitations (vibrational or rotational) that have been achieved in this work, and only data for low ro-vibrational excitations are presented in the literature. Previous effective Hamiltonian models for $^{12}C_2H_2$ (e.g., Ref. 37 or 35) have provided a good fit to experimental data obtained largely at room temperature but would not be expected to extrapolate so accurately up to high temperatures and thus do not offer the coverage that variational calculations do.

In order to test the (3*N*–5) implementation, an *ab initio* room-temperature spectrum of $^{12}C_2H_2$ was computed. This spectrum is not currently accurate enough for practical spectroscopic applications. Our experience shows (see, for example, Ref. 42) that the quality of the computational model can be substantially improved by fitting the PES of a molecule to the experimental energies or line positions. We are currently in the process of refining the *ab initio* PES of $^{12}C_2H_2$ presented here to the extensive set of experimentally determined energies of Ref. 41. This is expected to lead to a significant improvement in accuracy not only for the energies but also, as our preliminary results show, for intensities. Our aim is to produce an accurate line list for $^{12}C_2H_2$valid up to high temperatures of at least 1000 K, appropriate for the use in modeling hot exoplanet or cool stellar atmospheres, as part of the ExoMol project.[57,58]

SUPPLEMENTARY MATERIAL

See supplementary material for the files which are provided alongside this work. A description of each file is given in README.TXT.

ACKNOWLEDGMENTS

This work was supported by the ERC under Advanced Investigator Project No. 267219 and by STFC Project Nos. ST/M001334/1 and ST/J002925. The authors acknowledge the use of the UCL Legion High Performance Computing Facility (Legion@UCL), and associated support services, in the completion of this work, along with the Cambridge COSMOS SMP system, part of the STFC DiRAC HPC Facility supported by BIS National E-infrastructure capital Grant No. ST/J005673/1 and STFC Grant Nos. ST/H008586/1 and ST/K00333X/1. A.Y. acknowledges support from DESY (HGF IVF).

[1]M. Metsälä, F. M. Schmidt, M. Skytta, O. Vaittinen, and L. Halonen, J. Breath Res. **4**, 046003 (2010).
[2]A. Gaydon, *The Spectroscopy of Flames* (Springer Science & Business Media, 2012).
[3]E. E. Hughes and R. Gorden, Anal. Chem. **31**, 94 (1959).
[4]F. M. Schmidt, O. Vaittinen, M. Metsälä, P. Kraus, and L. Halonen, Appl. Phys. B **101**, 671 (2010).
[5]J. I. Moses, B. Bézard, E. Lellouch, G. Gladstone, H. Feuchtgruber, and M. Allen, Icarus **143**, 244 (2000).
[6]T. Encrenaz, M. Combes, S. K. Atreya, P. N. Romani, and K. Fricke, Astron. Astrophys. **162**, 317 (1986).
[7]S. T. Ridgway, Astrophys. J. **187**, L41 (1974).
[8]P. Drossart, B. Bézard, S. Atreya, J. Lacy, E. Serabyn, A. Tokunaga, and T. Encrenaz, Icarus **66**, 610 (1986).
[9]J. H. Waite, M. R. Combi, W.-H. Ip, T. E. Cravens, R. L. McNutt, W. Kasprzak, R. Yelle, J. Luhmann, H. Niemann, D. Gell, B. Magee, G. Fletcher, J. Lunine, and W.-L. Tseng, Science **311**, 1419 (2006).
[10]S. M. Hörst, J. Geophys. Res.: Planets **122**, 432, https://doi.org/10.1002/2016je005240 (2017).
[11]R. S. Oremland and M. A. Voytek, Astrobiology **8**, 45 (2008).
[12]T. Y. Brooke, A. T. Tokunaga, H. A. Weaver, J. Crovisier, D. Bockelée-Morvan, and D. Crisp, Nature **383**, 606 (1996).
[13]L. Le Roy, K. Altwegg, H. Balsiger, J.-J. Berthelier, A. Bieler, C. Briois, U. Calmonte, M. R. Combi, J. De Keyser, F. Dhooghe, B. Fiethe, S. A. Fuselier, S. Gasc, T. I. Gombosi, M. Hässig, A. Jäckel, M. Rubin, and C.-Y. Tzou, Astron. Astrophys. **583**, A1 (2015).
[14]S. T. Ridgway, D. N. B. Hall, S. G. Kleinmann, D. A. Weinberger, and R. S. Wojslaw, Nature **264**, 345 (1976).
[15]J. Tennyson and S. N. Yurchenko, Mol. Astrophys. **8**, 1 (2017).
[16]J. Tennyson and S. Yurchenko, Exp. Astron. **40**, 563 (2016).
[17]C. Bilger, P. Rimmer, and C. Helling, Mon. Not. R. Astron. Soc. **435**, 1888 (2013).
[18]H. Dhanoa and J. M. C. Rawlings, Mon. Not. R. Astron. Soc. **440**, 1786 (2014).
[19]U. G. Jørgensen, J. Hron, and R. Loidl, Astron. Astrophys. **356**, 253 (2000).
[20]J. Cernicharo, Astrophys. J. **608**, L41 (2004).
[21]M. Matsuura, P. R. Wood, G. C. Sloan, A. A. Zijlstra, J. T. van Loon, M. A. T. Groenewegen, J. A. D. L. Blommaert, M. R. L. Cioni, M. W. Feast, H. J. Habing, S. Hony, E. Lagadec, C. Loup, J. W. Menzies, L. B. F. M. Waters, and P. A. Whitelock, Mon. Not. R. Astron. Soc. **371**, 415 (2006).
[22]R. Gautschy-Loidl, S. Höfner, U. Jorgensen, and J. Hron, Astron. Astrophys. **422**, 289 (2004).
[23]R. Loidl, S. Höfner, U. G. Jørgensen, and B. Aringer, Astron. Astrophys. **342**, 531 (1999).
[24]B. Aringer, L. Girardi, W. Nowotny, P. Marigo, and M. T. Lederer, Astron. Astrophys. **503**, 913 (2009).
[25]A. Tsiaras, M. Rocchetto, I. P. Waldmann, G. Tinetti, R. Varley, G. Morello, E. J. Barton, S. N. Yurchenko, and J. Tennyson, Astrophys. J. **820**, 99 (2016).
[26]M. T. Lederer and B. Aringer, Astron. Astrophys. **494**, 403 (2009).
[27]P. Marigo and B. Aringer, Astron. Astrophys. **508**, 1539 (2009).
[28]U. G. Jørgensen, in *Molecules in Astrophysics: Probes and Processes: Proceedings of the 178th Symposium of the International Astronomical Union, Held in Leiden, The Netherlands, July 1–5, 1996* (Springer, 1997), includes index.
[29]M. J. Bramley and N. C. Handy, J. Chem. Phys. **98**, 1378 (1993).
[30]D. W. Schwenke, J. Phys. Chem. **100**, 2867 (1996).
[31]I. N. Kozin, M. M. Law, J. Tennyson, and J. M. Hutson, J. Chem. Phys. **122**, 064309 (2005).
[32]D. G. Xu, G. H. Li, D. Q. Xie, and H. Guo, Chem. Phys. Lett. **365**, 480 (2002).
[33]D. G. Xu, H. Guo, S. L. Zou, and J. M. Bowman, Chem. Phys. Lett. **377**, 582 (2003).
[34]A. Urru, I. N. Kozin, G. Mulas, B. J. Braams, and J. Tennyson, Mol. Phys. **108**, 1973 (2010).
[35]O. M. Lyulin and V. I. Perevalov, J. Quant. Spectrosc. Radiat. Transfer **201**, 94 (2017).
[36]O. M. Lyulin and A. Campargue, J. Quant. Spectrosc. Radiat. Transfer **203**, 461–471 (2017).
[37]B. Amyay, A. Fayt, M. Herman, and J. Vander Auwera, J. Phys. Chem. Ref. Data **45**, 023103 (2016).
[38]M. Herman, Mol. Phys. **105**, 2217 (2007).
[39]K. Didriche and M. Herman, Chem. Phys. Lett. **496**, 1 (2010).
[40]M. Herman, "High-resolution infrared spectroscopy of acetylene: Theoretical background and research trends," in *Handbook of High-Resolution Spectroscopy* (John Wiley & Sons, Ltd., 2011), pp. 1993–2026.

[41] K. L. Chubb, M. Joseph, J. Franklin, N. Choudhury, T. Furtenbacher, A. G. Császár, G. Gaspard, P. Oguoko, A. Kelly, S. N. Yurchenko, J. Tennyson, and C. Sousa-Silva, J. Quant. Spectrosc. Radiat. Transfer **204**, 42 (2018).
[42] S. N. Yurchenko and J. Tennyson, Mon. Not. R. Astron. Soc. **440**, 1649 (2014).
[43] S. N. Yurchenko, J. Tennyson, J. Bailey, M. D. J. Hollis, and G. Tinetti, Proc. Natl. Acad. Sci. U. S. A. **111**, 9379 (2014).
[44] S. N. Yurchenko, D. S. Amundsen, J. Tennyson, and I. P. Waldmann, Astron. Astrophys. **605**, A95 (2017).
[45] R. J. Barber, J. K. Strange, C. Hill, O. L. Polyansky, G. C. Mellau, S. N. Yurchenko, and J. Tennyson, Mon. Not. R. Astron. Soc. **437**, 1828 (2014).
[46] C. Sousa-Silva, A. F. Al-Refaie, J. Tennyson, and S. N. Yurchenko, Mon. Not. R. Astron. Soc. **446**, 2337 (2015).
[47] A. F. Al-Refaie, O. L. Polyansky, R. I. Ovsyannikov, J. Tennyson, and S. N. Yurchenko, Mon. Not. R. Astron. Soc. **461**, 1012 (2016).
[48] D. S. Underwood, J. Tennyson, S. N. Yurchenko, X. Huang, D. W. Schwenke, T. J. Lee, S. Clausen, and A. Fateev, Mon. Not. R. Astron. Soc. **459**, 3890 (2016).
[49] A. A. A. Azzam, S. N. Yurchenko, J. Tennyson, and O. V. Naumenko, Mon. Not. R. Astron. Soc. **460**, 4063 (2016).
[50] D. S. Underwood, J. Tennyson, S. N. Yurchenko, S. Clausen, and A. Fateev, Mon. Not. R. Astron. Soc. **462**, 4300 (2016).
[51] L. K. McKemmish, S. N. Yurchenko, and J. Tennyson, Mon. Not. R. Astron. Soc. **463**, 771 (2016).
[52] E. J. Zak, J. Tennyson, O. L. Polyansky, L. Lodi, N. F. Zobov, S. A. Tashkun, and V. I. Perevalov, J. Quant. Spectrosc. Radiat. Transfer **189**, 267 (2017).
[53] A. Owens, S. N. Yurchenko, A. Yachmenev, W. Thiel, and J. Tennyson, Mon. Not. R. Astron. Soc. **471**, 5025 (2017).
[54] S. N. Yurchenko, R. J. Barber, and J. Tennyson, Mon. Not. R. Astron. Soc. **413**, 1828 (2011).
[55] O. L. Polyansky, A. A. Kyuberis, L. Lodi, J. Tennyson, R. I. Ovsyannikov, and N. Zobov, Mon. Not. R. Astron. Soc. **466**, 1363 (2017).
[56] B. P. Mant, A. Yachmenev, J. Tennyson, and S. N. Yurchenko, Mon. Not. R. Astron. Soc. **478**, 3220 (2018).
[57] J. Tennyson and S. N. Yurchenko, Mon. Not. R. Astron. Soc. **425**, 21 (2012).
[58] J. Tennyson, S. N. Yurchenko, A. F. Al-Refaie, E. J. Barton, K. L. Chubb, P. A. Coles, S. Diamantopoulou, M. N. Gorman, C. Hill, A. Z. Lam, L. Lodi, L. K. McKemmish, Y. Na, A. Owens, O. L. Polyansky, T. Rivlin, C. Sousa-Silva, D. S. Underwood, A. Yachmenev, and E. Zak, J. Mol. Spectrosc. **327**, 73 (2016).
[59] I. E. Gordon, L. S. Rothman, C. Hill, R. V. Kochanov, Y. Tan, P. F. Bernath, M. Birk, V. Boudon, A. Campargue, K. V. Chance, B. J. Drouin, J.-M. Flaud, R. R. Gamache, J. T. Hodges, D. Jacquemart, V. I. Perevalov, A. Perrin, K. P. Shine, M.-A. H. Smith, J. Tennyson, G. C. Toon, H. Tran, V. G. Tyuterev, A. Barbe, A. G. Császár, V. M. Devi, T. Furtenbacher, J. J. Harrison, J.-M. Hartmann, A. Jolly, T. J. Johnson, T. Karman, I. Kleiner, A. A. Kyuberis, J. Loos, O. M. Lyulin, S. T. Massie, S. N. Mikhailenko, N. Moazzen-Ahmadi, H. S. P. Müller, O. V. Naumenko, A. V. Nikitin, O. L. Polyansky, M. Rey, M. Rotger, S. W. Sharpe, K. Sung, E. Starikova, S. A. Tashkun, J. Vander Auwera, G. Wagner, J. Wilzewski, P. Wcisło, S. Yu, and E. J. Zak, J. Quant. Spectrosc. Radiat. Transfer **203**, 3 (2017).
[60] L. S. Rothman, I. E. Gordon, R. J. Barber, H. Dothe, R. R. Gamache, A. Goldman, V. I. Perevalov, S. A. Tashkun, and J. Tennyson, J. Quant. Spectrosc. Radiat. Transfer **111**, 2139 (2010).
[61] H. S. P. Müller, F. Schlöder, J. Stutzki, and G. Winnewisser, J. Mol. Struct. **742**, 215 (2005).
[62] N. Jacquinet-Husson, R. Armante, N. A. Scott, A. Chédin, L. Crépeau, C. Boutammine, A. Bouhdaoui, C. Crevoisier, V. Capelle, C. Boonne, N. Poulet-Crovisier, A. Barbe, D. C. Benner, V. Boudon, L. R. Brown, J. Buldyreva, A. Campargue, L. H. Coudert, V. M. Devi, M. J. Down, B. J. Drouin, A. Fayt, C. Fittschen, J.-M. Flaud, R. R. Gamache, J. J. Harrison, C. Hill, Ø. Hodnebrog, S. M. Hu, D. Jacquemart, A. Jolly, E. Jiménez, N. N. Lavrentieva, A. W. Liu, L. Lodi, O. M. Lyulin, S. T. Massie, S. Mikhailenko, H. S. P. Müller, O. V. Naumenko, A. Nikitin, C. J. Nielsen, J. Orphal, V. I. Perevalov, A. Perrin, E. Polovtseva, A. Predoi-Cross, M. Rotger, A. A. Ruth, S. S. Yu, K. Sung, S. A. Tashkun, J. Tennyson, V. G. Tyuterev, J. Vander Auwera, B. A. Voronin, and A. Makie, J. Mol. Spectrosc. **327**, 31 (2016).
[63] M. Rey, A. V. Nikitin, Y. L. Babikov, and V. G. Tyuterev, J. Mol. Spectrosc. **327**, 138 (2016).
[64] S. N. Mikhailenko, Y. L. Babikov, and V. F. Golovko, Atmos. Oceanic Opt. **18**, 685 (2005).
[65] Y. A. Ba, C. Wenger, R. Surleau, V. Boudon, M. Rotger, L. Daumont, D. A. Bonhommeau, V. G. Tyuterev, and M.-L. Dubernet, J. Quant. Spectrosc. Radiat. Transfer **130**, 62 (2013).
[66] J. Tennyson and S. N. Yurchenko, Int. J. Quantum Chem. **117**, 92 (2017).
[67] S. N. Yurchenko, L. Lodi, J. Tennyson, and A. V. Stolyarov, Comput. Phys. Commun. **202**, 262 (2016).
[68] J. Tennyson, M. A. Kostin, P. Barletta, G. J. Harris, O. L. Polyansky, J. Ramanlal, and N. F. Zobov, Comput. Phys. Commun. **163**, 85 (2004).
[69] S. N. Yurchenko, W. Thiel, and P. Jensen, J. Mol. Spectrosc. **245**, 126 (2007).
[70] A. Yachmenev and S. N. Yurchenko, J. Chem. Phys. **143**, 014105 (2015).
[71] I. N. Kozin, M. M. Law, J. Tennyson, and J. M. Hutson, Comput. Phys. Commun. **163**, 117 (2004).
[72] S. Carter and N. C. Handy, Mol. Phys. **47**, 1445 (1982).
[73] M. J. Bramley, W. H. Green, and N. C. Handy, Mol. Phys. **73**, 1183 (1991).
[74] N. C. Handy, Mol. Phys. **61**, 207 (1987).
[75] S. Carter and N. C. Handy, Mol. Phys. **100**, 681 (2002).
[76] J. T. Hougen, P. R. Bunker, and J. W. C. Johns, J. Mol. Spectrosc. **34**, 136 (1970).
[77] B. T. Sutcliffe, in *Current Aspects of Quantum Chemistry*, Studies in Theoretical Chemistry, edited by R. Carbò (Elsevier, Amsterdam, 1981), p. 9.
[78] L. Halonen, M. S. Child, and S. Carter, Mol. Phys. **47**, 1097 (1982).
[79] J. Tennyson and B. T. Sutcliffe, Int. J. Quantum Chem. **42**, 941 (1992).
[80] B. T. Sutcliffe and J. Tennyson, Int. J. Quantum Chem. **39**, 183 (1991).
[81] A. B. McCoy and E. L. Sibert, J. Chem. Phys. **95**, 3476 (1991).
[82] S. Carter and N. Handy, Comput. Phys. Commun. **51**, 49 (1988).
[83] G. Brocks, A. van der Avoird, B. T. Sutcliffe, and J. Tennyson, Mol. Phys. **50**, 1025 (1983).
[84] P. Jensen, Comput. Phys. Rep. **1**, 1 (1983).
[85] P. Jensen, J. Mol. Spectrosc. **128**, 478 (1988).
[86] I. N. Kozin, M. M. Law, and J. Tennyson, Comput. Phys. Commun. **165**, 10 (2005).
[87] O. L. Polyansky, I. N. Kozin, P. Maĺyszek, J. Koput, J. Tennyson, and S. N. Yurchenko, J. Phys. Chem. A **117**, 7367 (2013).
[88] E. Zak, J. Tennyson, O. L. Polyansky, L. Lodi, S. A. Tashkun, and V. I. Perevalov, J. Quant. Spectrosc. Radiat. Transfer **177**, 31 (2016).
[89] J. K. G. Watson, Mol. Phys. **15**, 479 (1968).
[90] M. Rey, A. Nikitin, and V. Tyuterev, Mol. Phys. **108**, 2121 (2010).
[91] H. Romanowski, J. M. Bowman, and L. B. Harding, J. Chem. Phys. **82**, 4155 (1985).
[92] M. Rey, A. V. Nikitin, and V. G. Tyuterev, J. Chem. Phys. **136**, 244106 (2012).
[93] L. Hedberg and I. M. Mills, J. Mol. Spectrosc. **203**, 82 (2000).
[94] E. Mátyus, G. Czakó, B. T. Sutcliffe, and A. G. Császár, J. Chem. Phys. **127**, 084102 (2007).
[95] J. T. Hougen, J. Chem. Phys. **36**, 519 (1962).
[96] E. B. Wilson and J. B. Howard, J. Chem. Phys. **4**, 260 (1936).
[97] B. T. Darling and D. M. Dennison, Phys. Rev. **57**, 128 (1940).
[98] B. Podolsky, Phys. Rev. **32**, 0812 (1928).
[99] C. Eckart, Phys. Rev. **47**, 552 (1935).
[100] J. K. G. Watson, Mol. Phys. **19**, 465 (1970).
[101] P. R. Bunker and P. Jensen, *Molecular Symmetry and Spectroscopy*, 2nd ed. (NRC Research Press, Ottawa, Canada, 2006).
[102] G. O. Sørensen, in *Large Amplitude Motion in Molecules II*, Topics in Current Chemistry Vol. 82, edited by K. N. Houk *et al.* (Springer Berlin Heidelberg, Heidelberg, 1979), pp. 97–175.
[103] G. Strey and I. M. Mills, J. Mol. Spectrosc. **59**, 103 (1976).
[104] B. J. Howard and R. E. Moss, Mol. Phys. **20**, 147 (1971).
[105] J. K. G. Watson, Mol. Phys. **79**, 943 (1993).
[106] S. N. Yurchenko, A. Yachmenev, and R. I. Ovsyannikov, J. Chem. Theory Comput. **13**, 4368 (2017).
[107] K. L. Chubb, P. Jensen, and S. N. Yurchenko, Symmetry **10**, 137 (2018).
[108] G. Wlodarczak, "Linear polyatomic molecules: Introduction," in *Linear Polyatomic Molecules* (Springer Berlin Heidelberg, Berlin, Heidelberg, 2012), pp. 6–24.
[109] P. Jensen and P. Bunker, J. Mol. Spectrosc. **99**, 348 (1983).
[110] J. Tennyson and B. T. Sutcliffe, J. Mol. Spectrosc. **101**, 71 (1983).
[111] T. Hirano, U. Nagashima, and P. Jensen, J. Mol. Spectrosc. **343**, 54 (2018), spectroscopy of Large Amplitude Vibrational Motion, on the Occasion of Jon Hougen's 80th Birthday—Part II.
[112] T. Hirano, U. Nagashima, and P. Jensen, J. Mol. Spectrosc. **346**, 4 (2017).

[113]A. F. Al-Refaie, R. I. Ovsyannikov, O. L. Polyansky, S. N. Yurchenko, and J. Tennyson, J. Mol. Spectrosc. **318**, 84 (2015).
[114]I. Suzuki and J. Overend, Spectrochim. Acta, Part A **25**, 977 (1969).
[115]M. J. Bramley, S. Carter, N. C. Handy, and I. M. Mills, J. Mol. Spectrosc. **157**, 301 (1993).
[116]J. M. L. Martin, T. J. Lee, and P. R. Taylor, J. Chem. Phys. **108**, 676 (1998).
[117]W. D. Allen, Y. Yamaguchi, A. G. Császár, D. A. Clabo, R. B. Remington, and H. F. Schaefer, Chem. Phys. **145**, 427 (1990).
[118]S. L. Zou and J. M. Bowman, Chem. Phys. Lett. **368**, 421 (2003).
[119]S. Carter, I. M. Mills, and J. N. Murrell, Mol. Phys. **41**, 191 (1980).
[120]M. Herman, J. Lievin, J. Vander Auwera, and A. Campargue, *Global and Accurate Vibration Hamiltonians from High-Resolution Molecular Spectroscopy*, Advances in Chemical Physics Vol. 108 (Wiley and Sons, Inc., New York, NY, 1999).
[121]J. R. Alvarez-Collado, J. Mol. Struct.: THEOCHEM **433**, 69 (1998).
[122]H.-J. Werner, P. J. Knowles, G. Knizia, F. R. Manby, and M. Schütz, Wiley Interdiscip. Rev.: Comput. Mol. Sci. **2**, 242 (2012).
[123]C. Hätig, D. P. Tew, and A. Köhn, J. Chem. Phys. **132**, 231102 (2010).
[124]K. A. Peterson, T. B. Adler, and H.-J. Werner, J. Chem. Phys. **128**, 084102 (2008).
[125]H. Partridge and D. W. Schwenke, J. Chem. Phys. **106**, 4618 (1997).
[126]W. Kolòs and L. Wolniewicz, J. Chem. Phys. **41**, 3663 (1964).
[127]W. Kolòs and L. Wolniewicz, J. Chem. Phys. **49**, 404 (1968).
[128]A. Owens, S. N. Yurchenko, A. Yachmenev, J. Tennyson, and W. Thiel, J. Chem. Phys. **145**, 104305 (2016).
[129]A. G. Császár, Wiley Interdiscip. Rev.: Comput. Mol. Sci. **2**, 273 (2012).
[130]B. V. Noumerov, Mon. Not. R. Astron. Soc. **84**, 592 (1924).
[131]J. W. Cooley, Math. Comput. **15**, 363 (1961).
[132]M. Herman and J. Lievin, J. Chem. Educ. **59**, 17 (1982).
[133]D. Jacquemart, O. M. Lyulin, and V. I. Perevalov, J. Quant. Spectrosc. Radiat. Transfer **203**, 440 (2017).
[134]O. Lyulin, S. Béguier, S. Hu, and A. Campargue, J. Quant. Spectrosc. Radiat. Transfer **208**, 179 (2018).
[135]M. A. Temsamani, J. M. Champion, and S. Oss, J. Chem. Phys. **110**, 2893 (1999).
[136]J. Vander Auwera, D. Hurtmans, M. Carleer, and M. Herman, J. Mol. Spectrosc. **157**, 337 (1993).
[137]J. Vander Auwera, J. Mol. Spectrosc. **201**, 143 (2000).
[138]A. Kramida, Y. Ralchenko, and J. Reader, NIST atomic spectra database—Version 5, 2013, http://www.nist.gov/pml/data/asd.cfm.
[139]A. Owens, S. N. Yurchenko, A. Yachmenev, and W. Thiel, J. Chem. Phys. **143**, 244317 (2015).
[140]S. N. Yurchenko, R. J. Barber, J. Tennyson, W. Thiel, and P. Jensen, J. Mol. Spectrosc. **268**, 123 (2011).